Received: 28 March 2022 | Revised: 22 June 2022 | Accepted: 1 July 2022

DOI: 10.1002/ppp.2162

RESEARCH ARTICLE

WILEY

Thermokarst processes increase the supply of stabilizing surfaces and elements (Fe, Mn, Al, and Ca) for mineral–organic carbon interactions

Arthur Monhonval[1] | Jens Strauss[2] | Maxime Thomas[1] | Catherine Hirst[1] | Hugues Titeux[1] | Justin Louis[1] | Alexia Gilliot[1] | Eléonore du Bois d'Aische[1] | Benoît Pereira[1] | Aubry Vandeuren[1] | Guido Grosse[2,3] | Lutz Schirrmeister[2] | Loeka L. Jongejans[2,3] | Mathias Ulrich[4] | Sophie Opfergelt[1]

[1]Earth and Life Institute, Université catholique de Louvain, Louvain-la-Neuve, Belgium

[2]Permafrost Research Section, Alfred Wegener Institute Helmholtz Centre for Polar and Marine Research, Potsdam, Germany

[3]Institute of Geosciences, University of Potsdam, Potsdam, Germany

[4]Institute for Geography, Leipzig University, Leipzig, Germany

Correspondence
Arthur Monhonval, Earth and Life Institute, Université catholique de Louvain, Louvain-la-Neuve, Belgium.
Email: arthur.monhonval@uclouvain.be.

Present address
Mathias Ulrich, German Federal Environment Agency, Dessau-Roßlau, Germany.

Funding information
European Research Council; Fund for Scientific Research FNRS, Grant/Award Number: FC69480; European Union's Horizon 2020, Grant/Award Number: 714617

Abstract

The stabilizing properties of mineral–organic carbon (OC) interactions have been studied in many soil environments (temperate soils, podzol lateritic soils, and paddy soils). Recently, interest in their role in permafrost regions is increasing as permafrost was identified as a hotspot of change. In thawing ice-rich permafrost regions, such as the Yedoma domain, 327–466 Gt of frozen OC is buried in deep sediments. Interactions between minerals and OC are important because OC is located very near the mineral matrix. Mineral surfaces and elements could mitigate recent and future greenhouse gas emissions through physical and/or physicochemical protection of OC. The dynamic changes in redox and pH conditions associated with thermokarst lake formation and drainage trigger metal-oxide dissolution and precipitation, likely influencing OC stabilization and microbial mineralization. However, the influence of thermokarst processes on mineral–OC interactions remains poorly constrained. In this study, we aim to characterize Fe, Mn, Al, and Ca minerals and their potential protective role for OC. Total and selective extractions were used to assess the crystalline and amorphous oxides or complexed metal pools as well as the organic acids found within these pools. We analyzed four sediment cores from an ice-rich permafrost area in Central Yakutia, which were drilled (i) in undisturbed Yedoma uplands, (ii) beneath a recent lake formed within Yedoma deposits, (iii) in a drained thermokarst lake basin, and (iv) beneath a mature thermokarst lake from the early Holocene period. We find a decrease in the amount of reactive Fe, Mn, Al, and Ca in the deposits on lake formation (promoting reduction reactions), and this was largely balanced by an increase in the amount of reactive metals in the deposits on lake drainage (promoting oxidation reactions). We demonstrate an increase in the metal to C molar ratio on thermokarst process, which may indicate an increase in metal–C bindings and could provide a higher protective role against microbial mineralization of organic matter. Finally, we find that an increase in mineral–OC interactions corresponded to a decrease in CO_2 and CH_4 gas emissions on thermokarst process.

Mineral–OC interactions could mitigate greenhouse gas production from permafrost thaw as soon as lake drainage occurs.

KEYWORDS
Arctic, organic carbon stabilization, permafrost, redox processes, thaw, Yedoma

1 | INTRODUCTION

Permafrost deposits have been thawing at an unprecedented rate since the past century.[1–3] Climatic warming, which is two to three times more intense in northern regions, will accentuate permafrost thaw in the coming decades affecting the whole Arctic.[4] Therefore, the organic carbon (OC) stored in the permafrost deposits is mobilized. Even if a portion of the 1,300-Pg OC stock lying within permafrost regions[5,6] is decomposed upon thawing, this would result in significant greenhouse gas emissions at the global scale.[4] Thawing of Yedoma (i.e., ice-rich permafrost) deposits leads to massive landscape modifications.[7–9] The melting of ice-wedge networks and other excess ice usually leads to surface subsidence followed by thermokarst lake formation. With time, the lake can extend horizontally and vertically and eventually create a drainage pathway.[7] Upon lake drainage, sediment deposits remain within the dried basins, which are called "Alas." At the Arctic scale, lake and drained lake basin systems can represent up to about 50% of the circumpolar Northern Hemisphere permafrost region lowland areas.[10] About a quarter of the 21st-century thermokarst lake CH_4 release stems from newly thawed OC stored in deep deposits from the Yedoma region.[11] The thawing and draining of ice-rich deposits triggers shifts in soil or sediment properties, such as the reductive-oxidative potential (i.e., redox) or pH values. These shifts drive changes in biogeochemical processes with potential consequences for mineral–OC interactions (i.e., aggregation, organo-mineral associations, and organo-metallic complexes[12]) and thus OC mineralization rates.[10,13] These processes, leading to destabilization of these mineral–OC interactions, may accelerate permafrost carbon emissions and need to be incorporated in earth system models for more comprehensive projections of the permafrost carbon feedback.[3,14]

Mineral elements and mineral surfaces provide stabilizing mechanisms for OC resulting in the mitigation of OC mineralization in many soils.[12,13,15–22] OC-stabilizing mechanisms involving Fe and Al oxy (hydr)oxide have been extensively studied in (i) controlled conditions,[23–26] (ii) agricultural soils,[27] (iii) tropical lateritic soils,[28–30] (iv) peatlands and rice paddy soils,[31–34] and (v) lake and marine sediments.[35–37] However, more recently, there has been an increasing interest in permafrost regions.[38–46] In addition, Mn and Ca play a key role in OC stabilization and degradation mechanisms.[46–51] Overall, Fe-, Al-, Mn-, and Ca-bearing minerals and cations can provide physical and physicochemical protection of OC. For microbial mineralization, OC has to be in intimate contact with microorganisms. Physical protection of OC within mineral aggregates prevents microorganisms from approaching this substrate and thus limits this contact. Physicochemical protection, in the form of organo-mineral associations within clay or Fe-, Mn-, Al-(oxyhydr)oxides using polyvalent cation bridges such as Fe^{3+}, Al^{3+}, Ca^{2+}, and Mn^{3+} (adsorption) or in the form of organo-metallic complexes (Fe-, Mn-, Al-, and Ca-OC; complexation), hinders microbial degradation through diverse types of chemical bindings (e.g., von Lützow et al[13]). Overall, physical and physicochemical protection of OC through mineral–OC interactions lowers the solubility of organic acids and their availability for microorganisms.

A major concern is that mineral–OC interactions that promote OC stabilization could be highly reversible under changing physicochemical conditions, including both redox and pH[13,52,53] that occur during thermokarst processes. Fluctuating wet–dry cycles drive redox shifts in otherwise well-drained soils resulting in mineral dissolution, OC mobilization, and subsequent OC mineralization.[47,54–58] These shifts in redox potential influence redox-sensitive elements (i.e., Fe and Mn) by modifying the crystallinity of Fe- and Mn-oxy (hydr)oxides or the redistribution of stabilizing surfaces, with subsequent OC release.[29,43,45,59] The processes of wetting and drying are also evident in thawed lake basins. The reductive conditions induced on lake formation may have an opposite influence on mineral–OC interactions compared to the oxidative potential induced on lake drainage. Along the redox ladder (Figure 1), electron acceptors follow the sequence O_2, NO_3^-, NO_2^-, Mn^{4+}, Fe^{3+}, SO_4^-, and CO_2, which is more to less thermodynamically efficient. However, studies show that these redox reactions often overlap under environmental conditions (e.g., Kappler et al[55]). Besides the redox conditions, the pH is a key driver of Al-, Fe-, and Mn-oxy (hydr)oxide solubility and dissolution rates.[12] Furthermore, in soils/sediments with a high pH (neutral/alkaline), Ca promotes OC stabilization via aggregation, cation bridging, and/or complexation[13,51,60] and may also raise the surface potential of Fe-, Mn-, and Al-oxy-(hydr)oxides, which leads to more effective coagulation of OC.[61] The contribution of Ca to OC stabilization was even described in permafrost systems.[46] In soils with an acidic/neutral pH, the loss of Ca-based stabilizing mechanisms enables OC microbial degradation.[51]

Most mineral–OC interaction studies focus on one or a few elements involved in OC stabilization, but, to our knowledge, very few studies investigated Fe, Mn, Al, and Ca interactions with OC simultaneously. In ice-rich permafrost regions, interactions between minerals and OC are crucial given that most of the OC is found in deep mineral sediments, potentially enhancing interactions between the mineral and the organic compounds on thawing.[17,42,62] Although the increase in Fe-stabilizing surfaces from undisturbed (not thawed since deposition) Yedoma deposits to previously thawed Alas deposits was

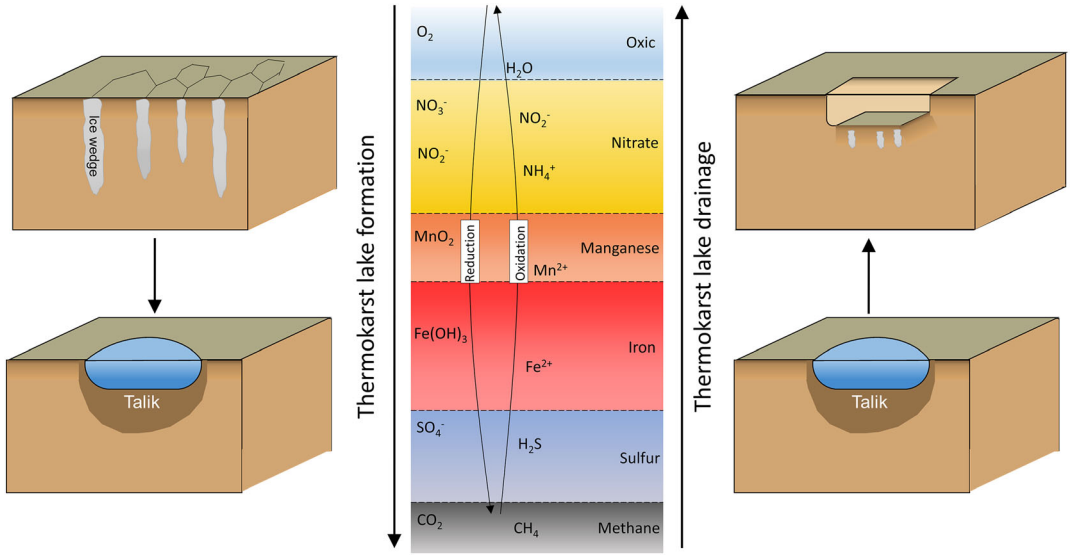

FIGURE 1 Simplified view of the oxidation–reduction couples involved in redox reactions and listed in thermodynamic order. The redox potential is decreasing toward the bottom of the column. On thermokarst lake formation (left), electron acceptors for reactions follow the sequence O_2, NO_3^-, MnO_2, Fe^{3+}, SO_4^-, and CO_2. On lake drainage (right), the redox potential increases and favors oxidation reactions. The colored panels indicate the sequence in which the different reactions are expected to occur based on thermodynamics; however, these redox reactions may overlap under environmental conditions (modified from Melton et al[64]) [Colour figure can be viewed at wileyonlinelibrary.com]

recently shown,[43] neither the influence of thermokarst lake formation and drainage on mineral–OC interactions in sediments nor the role of all potential reactive metals (Fe, Mn, Al, and Ca) was investigated. We hypothesize that lake formation and lake drainage are important intermediate steps controlling changes in mineral–OC interactions on thermokarst process, with likely opposing effects.

To test our hypothesis, we studied a landscape transect in Central Yakutia from undisturbed sediments in Yedoma uplands to drained lake sediments and sediments below thermokarst lakes from different generations.[63] The different thawing history of these deposits allows us to dissociate thermokarst lake formation on the one hand and thermokarst lake drainage and refreezing on the other hand. This comparison provides a glance into the evolution of ice-rich permafrost deposits in the near future and allows us to assess how mineral–OC interactions (with Fe, Mn, Al, and Ca) will evolve within the thawed, drained, and refrozen deposits.

2 | REGIONAL SETTINGS

Yukechi, the site studied, is located 80 km southeast from the city of Yakutsk in the central part of the Sakha (Yakut) Republic, East Siberia, Russia (Figure 2a). The region is characterized by a cold and continental climate with a mean annual temperature of −10.7°C (mean January: −41°C, mean July: 18.5°C) and a mean annual precipitation of 246 mm (period: 1982–2012; Yakutsk Weather Station: RSM00024959[65]). Between 1966 and 2016, the Central Yakutian mean annual air temperature increased by 0.3–0.6°C per decade.[66] Central Yakutia lies within the continuous permafrost zone and is in a low-relief landscape, characterized by numerous Alas basins and thermokarst lakes at different evolutionary stages,[67,68] indicating past and modern active thermokarst processes.[63]

The Yukechi site is located within the Yedoma domain.[9] The Yedoma deposits of this region can be more than 30 m thick.[67] For tens of millennia, cold and dry conditions during the late Pleistocene and continuous sedimentation led to the accumulation of several tens of meters thick Yedoma deposits with characteristic ice-wedge formation (I) (Figure 3a). These ice wedges formed by the infilling of vertical frost cracks with snow melt water repeatedly.[8] Warm and wet climate conditions during the Holocene period led to ice-wedge melting and a thermokarst lake formed within the subsidence area (II). With time, evaporation and thermokarst lake expansion in depth (i.e., talik deepening) or laterally (i.e., thermoerosion) led to the drainage of the thermokarst basin and consequent refreezing of the deposits (III).[7] Since the onset of the Holocene until now, lake formation and potential drainage have occurred within the refrozen Alas basin or within frozen Yedoma deposits (IV).

The studied transect included four evolutionary stages: undisturbed Yedoma sediments (Yedoma dry), sediments underneath a recently formed lake (Yedoma lake), Alas sediments in a drained thermokarst lake basin (Alas dry), and sediments underneath a lake in the drained basin which have been subject to multiple lake generations (Alas lake) (Figures 2b and 3b). The Yedoma lake is a recent lake that formed in Yedoma uplands about 70 years ago (Yedoma lake), defined here as initial lake formation (lake formation timeline observed by aerial photography from 1944 until today[63]). This recent thermokarst lake formation in the Yedoma uplands indicates ongoing thermokarst processes.[63,69] The Alas sediments experienced drainage/evaporation and refreezing in previous thermokarst lake generations.[70] In the following, we will split the thermokarst process using specific stages:

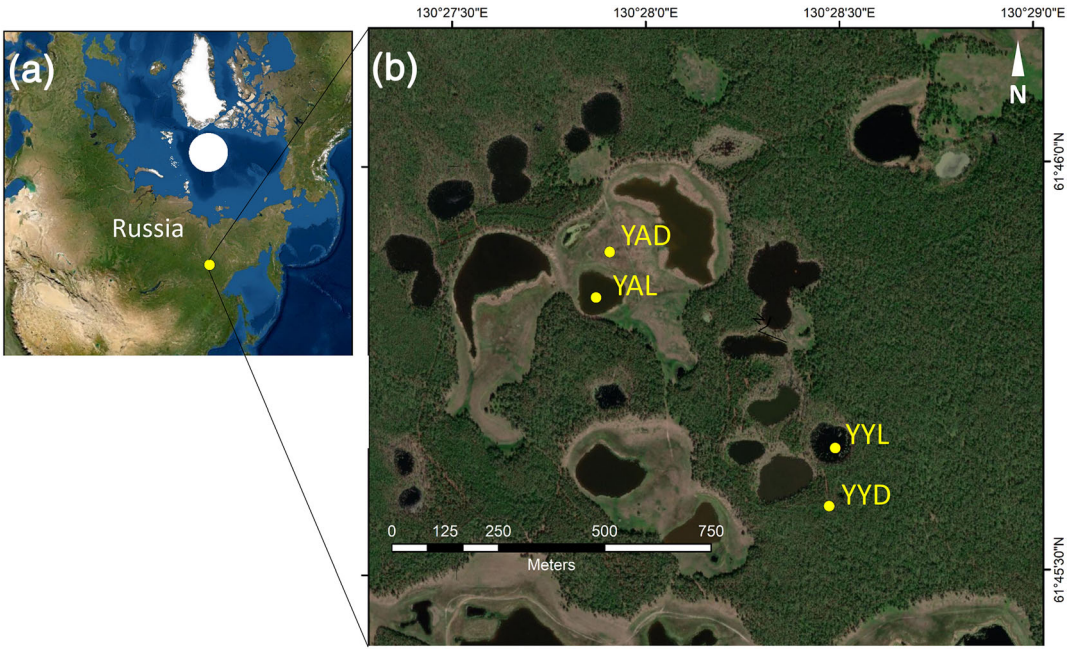

FIGURE 2 (a) Location of the Yukechi site in Russia. (b) Location of the four cores within Yukechi site: the Yedoma dry (YYD), the Yedoma lake (YYL), the Alas dry (YAD), and the Alas lake core (YAL). Source: Esri, DigitalGlobe, GeoEye, Earthstar Geographics, CNES/Airbus DS, USDA, USGS, AeroGRID, IGN, and the GIS User Community [Colour figure can be viewed at wileyonlinelibrary.com]

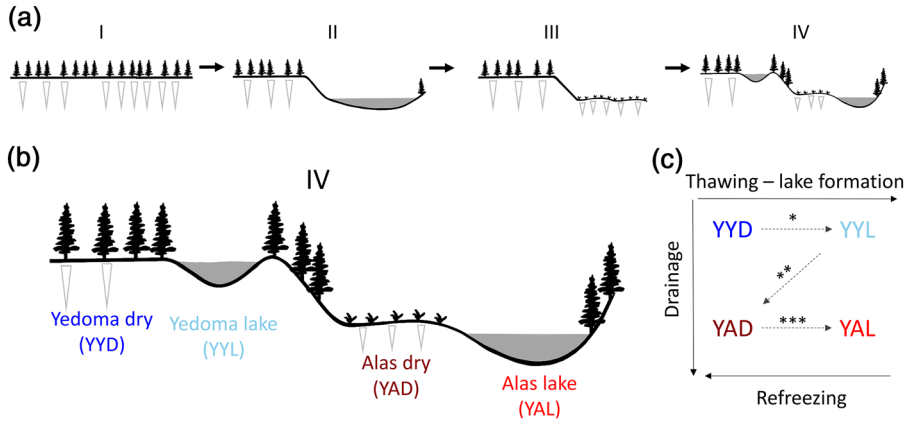

FIGURE 3 (a) Scheme of the permafrost degradation history (I–IV) of the site sampled in this study. Previous Yedoma uplands, with characteristic ice wedges (white triangles), have experienced the thermokarst process with thermokarst basin formation and drainage since the onset of the Holocene until now (I–III). More recently, about 70 years ago, a thermokarst lake formed in the Yedoma uplands (IV). (b) Sediment cores retrieved from the Yukechi site include a core from the Yedoma uplands (Yukechi Yedoma dry [YYD]), a core beneath a recent Yedoma lake (Yukechi Yedoma lake [YYL]), a core from a drained thermokarst lake basin (Yukechi Alas dry [YAD]), and a core beneath a mature Alas lake (Yukechi Alas lake [YAL]). (c) Permafrost degradation processes involved within each core: *thawing and initial lake formation, **drainage and refreezing, and ***secondary thawing and mature lake formation. The combination of initial lake formation (*) and drainage and refreezing (**) will be referred as the shift from Yedoma dry to Alas dry cores [Colour figure can be viewed at wileyonlinelibrary.com]

(i) thawing and initial lake formation (*), (ii) lake drainage and refreezing (**), and (iii) secondary thawing and mature lake formation (***) (Figure 3c). Yedoma and Alas deposits can be clearly subdivided into different stratigraphic units that reflect varying sedimentation processes confirmed by grain-size analysis, as described for the Yedoma dry and Alas dry cores[71] and for the Yedoma and Alas core beneath the lakes.[69,70]

3 | MATERIALS AND METHODS

3.1 | Coring and sample preparation

The field campaign to Yukechi was carried out in March 2015 to retrieve four sediment cores from different landform features (Section 2): a Yedoma dry core (YYD), a Yedoma lake core (YYL), an

Alas dry core (YAD), and an Alas lake core (YYL) (coordinates in Supplementary Table S1). Drilling was carried out using a URB2-4T drilling rig mounted on a truck. The cores drilled had a diameter of 15.7 cm in the uppermost parts and 8 cm in the lower parts. The sediment cores were removed from the core barrel using compressed air, described, stored in plastic bags, and kept frozen until laboratory analysis. The drilling depths below the surface (i.e., lake-ice surface for lake cores) were 22.4 m (YYD), 17.2 m (YYL), 19.8 m (YAD), and 17.7 m (YAL) (Supplementary Figure S1). On coring, the presence of taliks, that is, portions of the sediments that remain unfrozen during winter, sometimes led to partial core loss.[69,70] The Yedoma dry core included an ice wedge between 700 and 950 cm b.s. (below surface), and a talik section was identified between 100 and 200 cm b.s. The Yedoma lake core was frozen below 12 m, with significant core loss on core retrieval for the upper unfrozen section. In the Alas dry core, a talik was found between 160 and 750 cm b.s. The Alas lake core was unfrozen for the entire core. The frozen cores were split lengthwise using a band saw and were subsequently subsampled in a freezer room at −5°C (sample positions along the core are shown in Supplementary Figure S1). The samples were then air-dried before analyses. In total, 39 samples were analyzed in this study. The locations and numbers of samples analyzed are indicated in Supplementary Table S1.

3.2 | Sample characterization

3.2.1 | pH and mineralogy

Sample pH-H_2O and pH-KCl (1 M KCl solution) were measured on bulk sediment samples ($n = 39$) with a sediment to solution ratio of 1:5.[72] The pH was measured using a WTW Inlolab 720 pH-meter probe after 1 hour, with manual shaking every 20 minutes. Bulk sediment mineralogy was determined using X-ray diffraction (XRD, $n = 39$). The mineralogy of bulk samples was determined using finely ground powder (Cu-Kα, Bruker D8 Advance diffractometer, detection limit = 5%). Diffraction spectra were analyzed using DiffracPlus EVA software version 10.0.0.3 and PDF-2[73] and EVA-embedded DiffracPlus Reference databases (Mineral and Master data sets) using the peak fitting method.

3.2.2 | Total Fe, Mn, Al, and Ca concentration measurement

Total mineral element concentrations (Fe, Mn, Al, and Ca) were measured ($n = 39$) using a portable X-ray fluorescence (pXRF) device and corrected with inductively coupled plasma optical emission spectrometry (ICP-OES) measurement after alkaline fusion. This procedure is fully described in Monhonval et al[74] This procedure involves converting the raw pXRF element concentration values using a linear regression model to be equivalent to an ICP-OES concentration value obtained after alkaline fusion. Here, only pXRF concentration values corrected using element-specific regressions with high coefficient of determination ($R^2 > 0.72$) were used.

We performed pXRF measurements in the laboratory on dried samples to avoid variability of water content on measurements ($n = 39$).[75] For this, air- or freeze-dried samples were placed in a circular plastic cap (2.5-cm diameter) provided at its base with a transparent thin film (prolene 4 μm). Measurements were carried out using a pXRF device Niton XL3t GOLDD+ (Thermo Fisher Scientific, Waltham, USA) and a lead stand to protect the operator from X-rays. The total time of measurements was set to 90 seconds.[74]

For alkaline fusion used to calibrate the linear regression, air- or freeze-dried samples were ground in an agate mill. A portion (80 mg) of the milled sample was mixed with Li-metaborate and Li-tetraborate and heated for 10 minutes in a 1,000°C oven. The fusion bead was dissolved in HNO_3 2.2 N at 80°C and stirred until complete dissolution. We measured the mineral element concentrations in that solution using ICP-OES (iCAP 6500 Thermo Fisher Scientific, Waltham, USA). Loss on ignition was measured to evaluate the sum of oxides (between 98% and 102%), and the concentration values were reported in reference to the sediment dry weight (105°C). The ICP-OES method was performed on a subset of Yukechi samples ($n = 6$) to confirm that the linear regression from the Yedoma domain ($n = 144$)[74] was appropriate for Yukechi samples (Supplementary Figure S2).

3.2.3 | Selective Fe, Mn, Al, Ca, and OC extraction methods

Commonly used selective extraction methods were chosen to identify the Fe, Mn, Al, Ca, and OC phases. Fe, Mn, and Al were measured in a filtered solution (using a 20-μm Whatman 41 filter) by ICP-OES after the following extraction procedures: (i) dithionite-citrate-bicarbonate (DCB),[76] (ii) ammonium oxalate in the dark for 4 hours (oxalate),[77] and (iii) sodium pyrophosphate (pyrophosphate).[78] In soils/sediments with a high pH, Ca could be an important contributor to the stabilizing mechanisms affecting OC.[51,79] Therefore, we measured Ca concentrations within the pyrophosphate extract. Extraction methods using DCB, oxalate, and pyrophosphate are standard procedures to determine Fe- and Al-(oxyhydr)oxide phases or complexed ions (Supplementary Table S2). Here, we tested these extractions to decipher the different Mn phases. We found that the different extraction methods extracted different pools of Mn (Supplementary Figure S3). In addition, the Mn concentrations measured using ICP-OES on the solid residue after the different extractions confirm that DCB, oxalate, and pyrophosphate extractions target different Mn pools. Repetitions ($n = 3$) for three different samples were conducted to assess the precision of the different methods (Supplementary Table S3). This analysis supports that these extractions can also be used to assess Mn pools.

Extraction with DCB is presumed to remove well crystalline, poorly crystalline Fe oxides, and Fe complexed with organic matter from soil or sediment,[80] also called "free iron." Extraction with

dithionite reduces Fe (III) from oxides. Similarly, Mn (IV) should be reduced to Mn (II) since Mn is redox sensitive. The reduction of Mn (IV) is effective with hydroxylamine (NH_2OH), a weaker reductant than dithionite.[81] Therefore, we assume that dithionite reduces Mn (IV) within Mn oxides as well. Substantial amounts of Al and Ca are released via dithionite without targeting specific Al or Ca pools. The released Fe (II), Mn (II), and Al^{3+} and Ca^{2+} ions remain in solution and complex with citrate (complexing agent).

Extraction with oxalate at pH 3 targets poorly crystalline oxides and complexed forms. At pH <3.5, oxides are protonated weakening the metal–O bond, which is the first stage of dissolution, followed by the adsorption of oxalate and release of complexed Fe^{3+} and Al^{3+}. Oxalate extraction (4 hours in the dark) is a rate-limited process, which targets poorly crystalline phases and complexed metals, whereas longer procedures target more crystalline phases.[80] Unlike in DCB extraction, several Al-containing minerals are dissolved by oxalate. These include hydroxyl-interlayer Al, poorly crystalline Al oxides, allophane, imogolite, and other poorly crystalline aluminosilicates.[80] We emphasize that oxalate-extracted Ca cannot be discussed because of the precipitation of Ca with oxalate on extraction.

Pyrophosphate extraction at pH 10 chelates polyvalent cations and therefore targets metals (Fe, Mn, Al, and Ca) complexed with organic species. It has been reported that Na-pyrophosphate not only targets organically bonded Fe but also includes nanoparticulate poorly crystalline Fe oxides.[82] Therefore, the release of Fe and Al from small particles that have not complexed with soil organic acids is not excluded during pyrophosphate extraction.[80]

The well-crystallized (DCB-extracted) oxides are less reactive toward organic compounds because they provide less specific surface area than poorly crystalline oxides.[83,84] Moreover, DCB-extracted Al cannot be attributed to distinct Al minerals and does not target well-crystalized Al oxides.[80] Dithionite extraction was also reported to be unexpectedly less efficient within some permafrost soils.[85] Because it is difficult to decipher which phases are extracted by using DCB extraction method, we define our "reactive" pool (i.e., the pool highly reactive toward organic species) by the pool extracted by ammonium oxalate. This pool should combine all poorly crystalline, amorphous, and complexed pools of Fe, Mn, and Al. Similarly, we define our reactive Ca as the pyrophosphate-extracted Ca because of the disadvantage attributed to Ca oxalate precipitation and should include Ca under complexed forms or interacting via cation bridging.

OC was quantified in oxalate and pyrophosphate extracts. The optical density of oxalate extract (ODOE), considered as an indicator of reactive polyaromatic acid concentration, was measured by determining the absorbance at 430 nm on a Genesys 10 S VIS spectrophotometer, with ammonium oxalate reagent as a blank.[86] Note that direct measurement of OC within the oxalate extract is not possible because of the organic composition of oxalate. From the pyrophosphate extract, the concentration in dissolved OC released after dispersion by pyrophosphate (referred as *Cp*) was measured using a Shimadzu total organic carbon analyzer (measuring nonpurgeable OC). This indicates the amounts of C involved in organo-metallic complexes in soils or sediments.[78] Repetitions ($n = 3$) for three different samples were conducted to assess the precision of the method (Supplementary Table S3).

3.3 | Statistical analysis

The Wilcoxon test (two sided) was used to assess statistical differences within reactive metals and organic compounds (C_p) between the different cores. In addition, correlation matrices using Pearson's method were constructed using *corrplot* package, performed using R software version 4.1.1.[87]

4 | RESULTS

4.1 | Sediment core pH and mineralogy

pH-H_2O ranged between 8.22 and 10.05 with a mean of 8.97, and pH-KCl ranged between 7.61 and 8.73 (mean = 8.18) (Supplementary Figure S4). Diffractograms indicate the presence of quartz, plagioclase, mica, pyroxene, amphibole, dolomite, serpentine, and vermiculite (Supplementary Table S4). Mineral phases below 5% may be present but are undetected.

4.2 | Total and selectively extracted Fe, Mn, Al, and Ca concentrations in sediment cores

The mean (±standard deviation) total concentrations in Fe, Al, and Mn among all studied sediment cores are 26.1 ± 4.9, 64.5 ± 5.2, and 0.50 ± 0.10 g kg^{-1}, respectively. Total Ca concentration reaches 23.6 ± 6.8 g kg^{-1}. Total Al concentration is two to three times higher than Fe concentrations and more than two orders of magnitude higher than Mn concentrations on mass concentration basis. The DCB-extracted Fe (mean: 5.41 g kg^{-1}) is almost one order of magnitude greater than DCB-extracted Al (mean: 0.63 g kg^{-1}), which is about twice greater than Mn (mean: 0.28 g kg^{-1}). Reactive Fe, Mn, and Al (defined here as oxalate-extracted pool) represent about 12% (3.3 g kg^{-1}), 28% (0.15 g kg^{-1}), and 1.3% (0.85 g kg^{-1}) of the bulk total concentration, respectively (Figure 4a). Finally, pyrophosphate-extracted Fe represents about 3% (0.82 g kg^{-1}) of total Fe. Pyrophosphate-extracted Mn (0.13 g kg^{-1}) and Al (0.10 g kg^{-1}) concentrations are smaller compared to Fe but are within the same order of magnitude and represent about 25% and 0.2%, respectively, of total Mn and total Al (Figure 4b). Pyrophosphate-extracted Ca shows the highest concentration with a mean of 3.5 g kg^{-1}.

When the differences in the selective extractions between the four stages of thermokarst formation were studied (Figure 2), we found that reactive (i.e., oxalate-extracted) Fe concentrations show a significant increase between Yedoma and Alas deposits

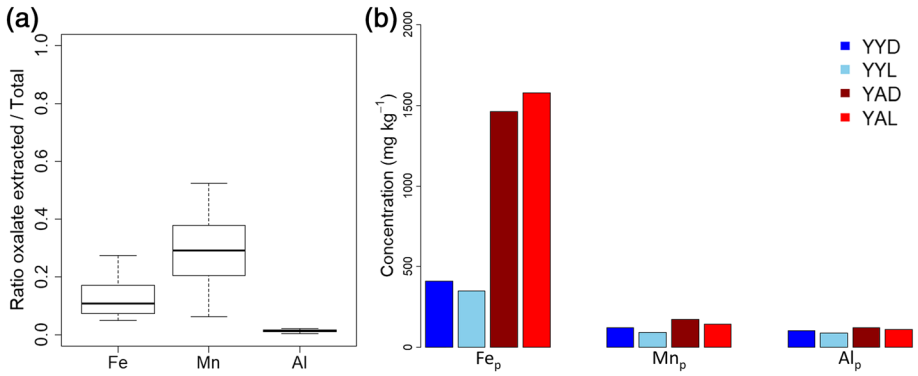

FIGURE 4 (a) Boxplot of the ratio between oxalate-extracted (i.e., reactive) and total Fe, Mn, and Al. (b) Histogram of mean concentrations in pyrophosphate-extracted Fe, Mn, and Al in the four sediment cores: Yedoma dry (YYD), Yedoma lake (YYL), Alas dry (YAD), and Alas lake (YAL) [Colour figure can be viewed at wileyonlinelibrary.com]

(Wilcoxon test p-value <0.05) but similar concentrations between dry and lake cores (p-value = 0.19). Similarly, reactive Mn shows significantly higher concentrations in the Alas compared to Yedoma core but significantly higher concentrations in dry deposits compared to lake deposits (Figure 5b). Reactive Al concentrations show a similar trend to reactive Mn, with higher concentrations in Alas cores compared to Yedoma cores and higher concentration in dry deposits than in lake deposits. Mean reactive Mn and Al concentrations are therefore the lowest in the Yedoma lake core and the highest in the Alas dry core. Oxalate-extracted Al concentration is higher than DCB-extracted Al (Figure 5c). Pyrophosphate-extracted Fe showed smaller concentrations in the Yedoma dry and Yedoma lake cores (mean: 0.41 and 0.35 g kg^{-1}) compared to the Alas dry and Alas lake cores (mean: 1.5 and 1.6 g kg^{-1}). This difference between Yedoma and Alas sediments is smaller for Mn and Al concentrations within pyrophosphate extraction (Figure 5). Pyrophosphate-extracted Mn concentrations are within the same order of magnitude as pyrophosphate-extracted Al (mean: 0.13 and 0.10 g kg^{-1}, respectively; Figure 4a) despite the huge difference (more than two orders of magnitude) in the bulk Al and Mn total concentrations in the sediments (Figure 5). Pyrophosphate-extracted Ca ranges from 0.542 and 6.86 g kg^{-1}, with mean values decreasing from Alas dry (4.40 g kg^{-1}), Alas lake (4.26 g kg^{-1}), Yedoma dry (3.06 g kg^{-1}) to Yedoma lake (2.89 g kg^{-1}) cores. Pyrophosphate-extracted Ca concentrations show higher values than the sum of pyrophosphate-extracted Fe, Mn, and Al combined.

Detailed graphs of the Fe, Mn, and Al concentrations over depth can be found in the supplements: total, DCB, oxalate, and pyrophosphate extractions (Supplementary Figures S5–S7) and total and pyrophosphate-extracted Ca (Supplementary Figure S8). Overall, DCB-, oxalate-, and pyrophosphate-extracted Fe and Mn follow the same pattern as their total concentration profile. The Al total concentrations are two to three orders of magnitude higher than the concentration of selectively extracted Al. The sandy layer present in the Yedoma dry (between 19.3 and 10.1 m b.s.) is within the low range of values for all elements for their total, DCB-extracted, oxalate-extracted, and pyrophosphate-extracted concentrations contributing to greater variability (i.e., wider boxplot) within the Yedoma dry core (Figure 5). The total and selectively extracted Fe, Mn, Al, and Ca concentrations are presented in Supplementary Data.

4.3 | Selective OC extractions

Pyrophosphate-extracted C (C_p) concentration ranges are 2.2–15.4 g kg^{-1} (YYD), 1.6–6.6 g kg^{-1} (YYL), 4.1–9.2 g kg^{-1} (YAD), and 4.0–6.2 g kg^{-1} (YAL) (Figure 6a). ODOE ranges are 0.014–0.161 (YYD), 0.021–0.056 (YYL), 0.025–0.087 (YAD), and 0.049–0.106 (YAL) (Figure 6b). The Yedoma dry core shows the wider range of pyrophosphate-extracted C concentrations and Alas lake the narrower range (Figure 6a). Pyrophosphate-extracted C and ODOE are positively correlated in the lower part of the Yedoma dry core ($R^2 = 0.52$) but not in the upper part (Supplementary Figure S9). The ODOE shows maximum values in the upper part of the Yedoma dry core. Notably, the sandy layer of the Yedoma dry core displays low-range values for pyrophosphate-extracted C and ODOE (Figure 6; Supplementary Figure S9). Absorbance and concentrations for selective carbon extractions are presented in Supplementary Data.

4.4 | Statistical analysis of reactive metal and organic variables between stages of thermokarst process

Statistical analyses between the different cores highlight significant differences at each stage of the thermokarst process (Table 1). The initial lake formation (YYD to YYL; see Figure 3) triggered minor changes (not statistically significant; p-value >0.05) in the concentration of the reactive metals (Fe_o, Mn_o, Al_o, and Ca_p) and organic compounds (C_p and ODOE) (Table 1). The most significant differences during these stages are an increase in the concentration of reactive Fe phases and a decrease in complexed C (p-value slightly higher than 0.05 threshold). Note that the average concentration of complexed C decreases significantly (p-value <0.05) when the sandy sediments from the Yedoma dry core are discarded. In comparison, the drainage and refreezing stages (YYL to YAD; Figure 3) show a statistically significant change for every parameter (p-value <0.05; Table 1): the concentration of all reactive metals (Supplementary Figure S10) and organic compounds (ODOE and C_p) increased significantly. Secondary thawing and mature lake formation (YAD to YAL; Figure 3) triggered significant changes only on the reactive Mn but had no significant effect on reactive Fe and Al nor on OC parameters (Figure 5; Table 1).

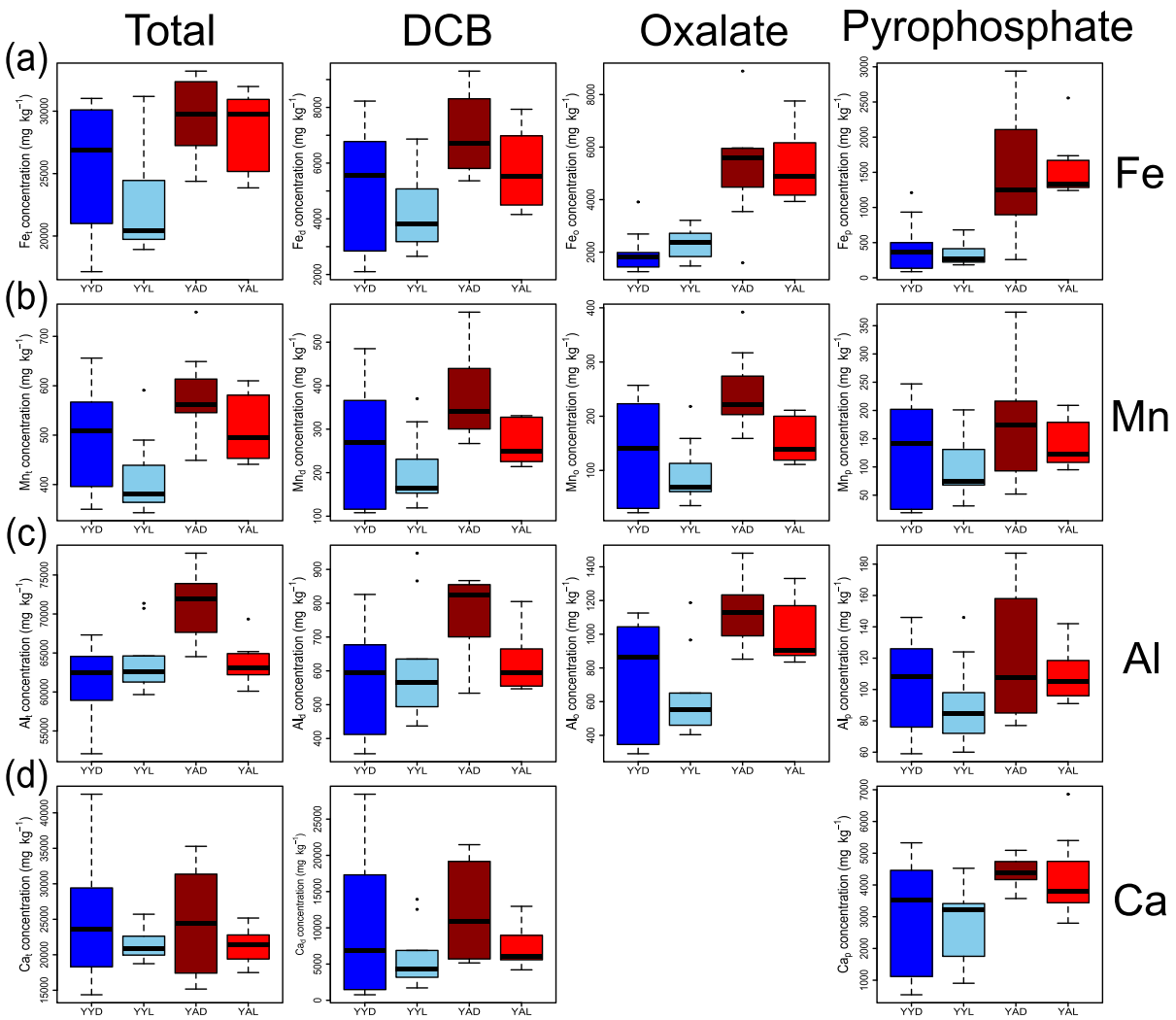

FIGURE 5 Boxplot of mineral element total concentrations and selectively extracted concentrations (expressed in mg kg^{-1}) using dithionite-citrate-bicarbonate (DCB), ammonium oxalate (oxalate), and Na-pyrophosphate (pyrophosphate) for (a) Fe, (b) Mn, (c) Al, and (d) Ca for the four cores in Yukechi: Yedoma dry (YYD), Yedoma lake (YYL), Alas dry (YAD), and Alas lake (YAL). Oxalate extraction of Ca is not shown due to precipitation issue (see Section 3.2.3). Yedoma cores are shown in blue and Alas cores in red. Indices are used for total, DCB, oxalate-, and pyrophosphate-extracted metals, for instance in panel (a): Fe_t, Fe_d, Fe_o, and Fe_p, respectively. Note that the Y-scaling differs between plots for all elements [Colour figure can be viewed at wileyonlinelibrary.com]

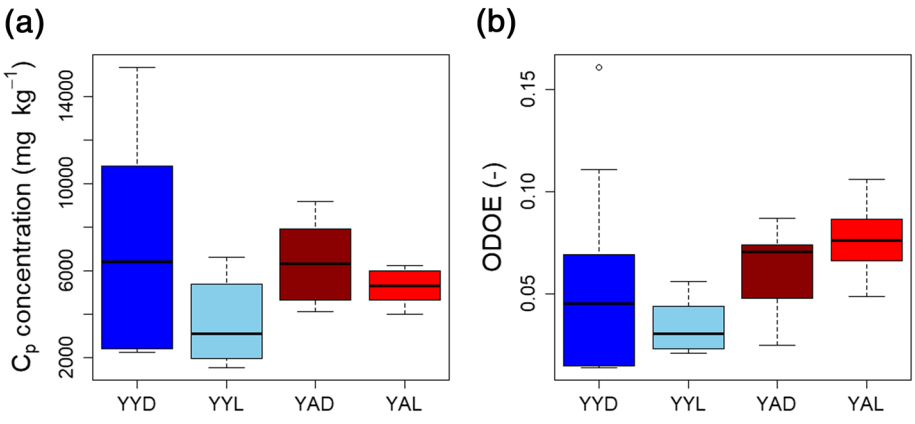

FIGURE 6 Boxplot of (a) pyrophosphate-extracted carbon concentration (C_p in mg kg^{-1}) and (b) optical density of the oxalate extract (ODOE) for Yedoma dry (YYD), Yedoma lake (YYL), Alas dry (YAD), and Alas lake (YAL) cores in Yukechi. Yedoma cores are shown in blue and Alas cores in red [Colour figure can be viewed at wileyonlinelibrary.com]

In sum, the evolution from the Yedoma dry to the Alas dry (YYD to YAD) shows a significant increase in the concentration of reactive Fe, Mn, and Al and no significant change for the other parameters (e.g., ODOE and C_p). The shift from Yedoma (YYD and YYL) to Alas (YAD and YAL) modifies the concentrations of reactive Fe, Mn, Al, and Ca (Table 1; Supplementary Figure S10). However, the shift from dry deposits (YYD and YAD) to deposits beneath lakes (YYL and YAL) significantly affects only reactive Mn and complexed C (Table 1; *p*-value <0.05). We found that all reactive metals are positively correlated with complexed C (Figure 7). Complexed Fe, which is the most abundant after Ca (Fe_p mean: 0.82 g kg^{-1}), shows the smallest correlation with complexed C ($r = 0.29$). On the contrary, complexed Mn (mean: ~0.13 g kg^{-1}), which is the least abundant along with Al, shows the highest correlation with pyrophosphate-extracted C ($r = 0.74$).

5 | DISCUSSION

5.1 | A typical Yedoma site modified by thermokarst process

Total mean Fe concentrations from all Yukechi cores (26.1 ± 4.9 g kg^{-1}, $n = 39$) are in the lower range of values compared to the median Fe concentration (31.7 ± 4.6 g kg^{-1}, $n = 1{,}292$) reported

TABLE 1 *p*-Value table of Wilcoxon test (two sided) to decipher statistical significance of subsets for reactive metals and organic compounds

	Fe_o	Mn_o	Al_o	Ca_p	ODOE	C_p
YYD versus YYL[a]	0.0841	0.285	0.371	0.709	0.598	0.074
YYL versus YAD[b]	**<0.05 (+)**	**<0.05 (+)**	**<0.05 (+)**	**<0.05 (+)**	**<0.05 (+)**	**<0.05 (+)**
YAD versus YAL[c]	0.955	**<0.05 (−)**	0.336	0.336	0.148	0.397
YYD versus YAD[d]	**<0.05 (+)**	**<0.05 (+)**	**<0.05 (+)**	0.110	0.171	0.868
Yedoma versus Alas	**<0.05 (+)**	**<0.05 (+)**	**<0.05 (+)**	**<0.05 (+)**	**<0.05 (+)**	0.352
Dry versus Lake	0.190	**<0.05 (−)**	0.292	0.305	0.910	**<0.05 (−)**

Notes. These reactive metals gather oxalate-extracted Fe, Mn, and Al (Fe_o, Mn_o, and Al_o) and pyrophosphate-extracted Ca (Ca_p). Organic compounds are presented for optical density of oxalate extract (ODOE) and pyrophosphate-extracted C (C_p). The *p*-values in bold font show statistically significant differences between the subsets. Subsets are the Yedoma dry (YYD), Yedoma lake (YYL), Alas dry (YAD), and Alas lake (YAL) cores. (+) or (−) represents whether the statistical difference is an increase or a decrease, respectively. ODOE, optical density of oxalate extract.

[a]Initial lake formation effect (Figure 3c; *)

[b]Drainage and refreezing effect (Figure 3c; **)

[c]Second lake formation effect (Figure 3c; ***)

[d]Lake formation and drainage effects (combination of footnotes a and b; ****).

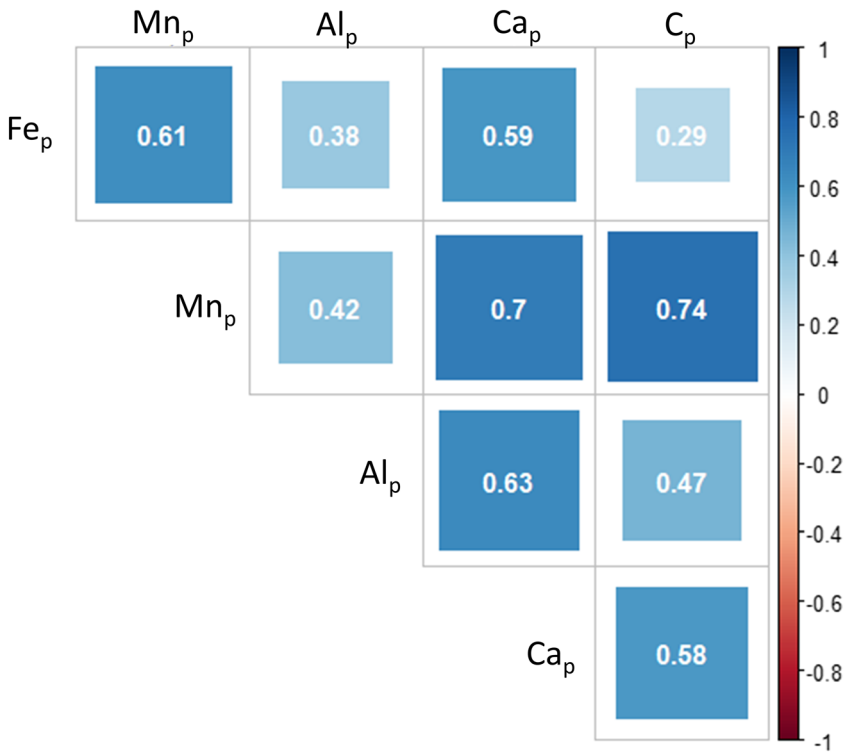

FIGURE 7 Upper correlation matrix using Pearson's method of complexed (pyrophosphate-extracted) metals and organic carbon ($n = 39$). Correlation matrix with all parameters, including total, dithionite-extracted, oxalate-extracted, and pyrophosphate- extracted metals, and C, is available in Supplementary Figure S11 [Colour figure can be viewed at wileyonlinelibrary.com]

throughout the Yedoma domain.[43] However, total mean Al and Mn concentrations are in the same concentration range (Al = 66.5 ± 6.9 g kg^{-1}; Mn = 0.498 ± 0.119 g kg^{-1}), as presented by Monhonval et al[88] in the Yedoma domain Mineral Concentration Assessment (YMCA) data set. The total mean Ca concentration is twice as high (23.6 ± 6.8 g kg^{-1}) as the Yedoma domain median value (10.4 ± 4.7 g kg^{-1}, n = 1,292).[74] Indeed, previous studies from Central Yakutia showed that deposits in the area are rich in carbonates.[89] This is further confirmed by the YMCA data set,[88] which highlights that Yukechi samples lie within the upper range of Ca concentration in Siberia (Supplementary Figure S12). The high pH values measured in Yukechi cores match previous findings from Central Yakutian lakes with a pH range of 7–10[90] and in unconnected Alas lakes from Central Yakutia with a pH >9.[91] Despite the fact that carbonate presence was undetected using the XRD method, reaction of the samples to HCl confirms the presence of calcite or other carbonates (including Na_2CO_3 if sample pH is above 9), which were previously reported in the area.[89] The carbonate presence within the Yukechi deposits, the high pH values reported within our four cores, and the high-range total Ca concentration emphasize that Ca is likely to be an important contributor for mineral–OC interactions.[46,51] Since redox and pH (to a lower extent) conditions can vary depending on the thawing history of deposits from each core, modifications in the contribution of each metal (Fe, Mn, Al, and Ca) to mineral–OC interactions are expected.

To confirm the findings of this space-for-time study design, the following assumptions about the four stages of thermokarst development are made. Within typical Yedoma deposits, there are a uniform mineralogical composition[6] and little postdepositional processing.[69] Previous work from Schirrmeister et al,[8,92] in the Yedoma domain confirms this assumption, showing that the Yedoma deposits originated from local sources and a variety of transport mechanisms, which resulted in a polygenetic formation of Yedoma deposits. We further assume that Alas deposits formed within and from Yedoma deposits are mainly composed of relocated and reworked Yedoma sediments,[93] although authigenic deposition on lake formation and drainage is expected. The uniform mineralogical nature of the Yukechi site is confirmed by the similarity of detected crystalline minerals from XRD analyses within the original Yedoma dry cores and within the other three cores (Supplementary Table S4). The variety of transport mechanisms is confirmed by different grain-size distributions reported in previous studies.[69,71,89] Therefore, we expect the main changes in mineral–OC interactions (i.e., Fe-, Mn-, and Al-oxy (hydr)oxides and Fe, Mn, Al, and Ca complexes and their associations to organic compounds) to be related to changing physicochemical conditions in the sediment (i.e., redox state and pH), on thermokarst processes and not related to a different composition of the original deposit. However, we acknowledge that spatial heterogeneity of the Yukechi site was not investigated and might explain part of the discrepancies observed in Yedoma and Alas deposits subjected to previous thaw. We acknowledge that additional factors not considered here, such as the diversity of microbial communities (e.g., modulating CO_2:CH_4 or oxide dissolution rates), the spatial and functional complexity in the sediment (e.g., the structuring of space into a network of more or less connected microsites that determine local environment conditions), or the catalyst role of mineral elements for organic reactions (e.g., through the creation of center of reactivity, proton transfer, or electron acceptor), may also contribute to influence mineral–OC interactions to some extent.[56]

5.2 | Decoupling the influence of lake formation and lake drainage on mineral–OC interactions

Biogeochemical conditions in the sediment (referring to redox and pH) are modified during lake formation and lake drainage.[57] Lake formation and lake drainage may lead to contrasted physicochemical conditions for OC stabilization and modify mineral–OC interactions. Indeed, mineral elements involved in mineral–OC interactions are either redox sensitive (Fe and Mn) and/or pH sensitive (Fe, Mn, Al, and Ca). We assume redox conditions to change significantly beneath lakes or in dry deposits.[32,57] However, the pH measured within the four cores (dry and lake cores) displays high values (~8) without significant differences between cores, which complicates the observation of modifications for pH-sensitive elements. Combining our data of the four sediment cores, we are able to dissociate the impact of the following stages on mineral–OC interactions in the Yukechi sediments: (i) initial lake formation (modifications between the Yedoma dry and Yedoma lake cores); (ii) lake drainage and partial refreezing (modifications between the Yedoma lake and Alas dry cores); and (iii) second/mature lake formation (modifications between the Alas dry and Alas lake cores).

The difference in reactive Fe, Mn, and Al across the Yedoma and Alas sites shows that there are opposing mechanisms on lake formation and lake drainage. We demonstrate that the processes occurring during the intermediate steps are masked when comparing only the initial (YYD) and the final (YAD) deposit stage resulting from thermokarst processes. For instance, we observe that the combination of initial lake formation and drainage (YYD to YAD) shows no significant differences within the organic parameter concentrations (Table 1, footnote d). Nonetheless, when considered separately, there is a decrease in lake formation followed by an increase in lake drainage for most parameters, including reactive metals, ODOE, and C_p. We highlight that initial (*, Figure 3b) and secondary (***, Figure 3b) stages of lake formation had only minor effects on pedogenic Fe, Mn, Al, and Ca but greater effects on OC phases (Table 1). On the contrary, drainage and refreezing (**, Figure 3b) of the Alas dry formation corresponded to a significant increase in reactive metal (Fe, Mn, Al, and Ca) oxides and complexes and also a significant increase in ODOE and C_p. We can therefore state that reactive mineral formation and OC stabilization during drainage and refreezing outweigh any reactive mineral and OC loss during the first thermokarst stage (i.e., initial lake formation). This finding confirms that organic acid concentrations are unchanged between the Yedoma dry and the Alas dry core (e.g., p-value = 0.87 for C_p). However, the intermediate stages involved in the formation of the Alas dry may have changed the form and properties of mineral–OC interactions from the original deposit

with an increase in the potential to stabilize OC. Consequently, the Alas dry core contained the largest pool size of DCB-extracted Fe and Mn and the highest reactive Fe and Mn proportion within this pool (Figure 8). More specifically, the size of the DCB-extracted pool increased about 36% for both Fe and Mn between the Yedoma dry and the Alas dry core. Reactive (amorphous and complexed) Fe increased from 37% to 75%, and Mn increased from 51% to 65% of the DCB-extracted pool (Figure 8).

The proportion of crystalline, amorphous, and complexed Fe and Mn phases evolve with lake formation and lake drainage (Figure 8). Between the least degraded (Yedoma dry, YYD) and the more degraded core (Alas lake, YAL), the total DCB-extracted pool is relatively unchanged (increase of 11% for Fe and decrease of 1.5% for Mn). However, when we studied the distribution of Fe and Mn between the reactive phases, we observed some differences. First, for Fe, the proportion of the complexed Fe phases increased threefold, and the amorphous Fe phases doubled at the expense of the proportion of crystalline phases that decreased significantly (63% of the dithionite-extracted pool in Yedoma dry to 8% in the Alas lake). More specifically, in the least degraded Yedoma dry core, the majority of the DCB-extracted Fe was present as crystalline phases (63%) followed by amorphous pool (29%) and complexed phases (8%) (Figure 8). The Alas lake sediment core shows a very distinct distribution of the different Fe pools, with only 8% of the DCB-extracted Fe as crystalline phases and an increase of 65% of amorphous phases and 27% of complexed forms. Second, for Mn, the crystalline phases represent 50%, the amorphous only 5.5%, and complexed forms 44.5% of the DCB-extracted pool in the Yedoma dry core. The Alas lake shows a small depletion in crystalline phases (42%), amorphous phases stay unchanged (5%), and complexed forms increase (53%) in the DCB-extracted Mn pool (Figure 8). Overall, this confirms a significant shift toward less crystalline and more reactive (amorphous and complexed) Fe compounds between the initial and the final steps considered and only a slight shift for reactive Mn compounds.

The decrease in reactive Mn on lake formation (Figure 5b), which is not the case for reactive Fe (Figure 5a), was not expected. Indeed, their similar properties related to redox sensitivity would suggest that both reactive Mn and Fe would increase on oxidative conditions and decrease on reductive conditions. We propose that water saturation of Alas deposits beneath the lake might have decreased the redox potential only to a certain extent. To confirm this assumption, Hughes-Allen et al[91] observed a decrease in dissolved O_2 to below 5% during winter in the bottom of shallow (~2 m deep) unconnected lakes from Central Yakutia (located less than 100 km apart and with very similar properties as the lakes overlying Yedoma and Alas lake cores from this study). The depleted oxygen levels beneath those lakes are additional evidence for a lower redox potential in the below-lake deposits discussed here. According to the redox ladder (Figure 1), Mn species are thermodynamically more favorable to reduce before Fe reduction. This means that Mn is theoretically reduced before Fe species on reduction and Fe should be oxidized before Mn species on oxidation.[55,94] As a consequence, reduction in Mn minerals may be spatially separated from reduction in Fe minerals (e.g., in stratified lake sediments).[55] The potential Mn reduction on lake formation might have a protective effect on Fe reduction and prevent reactive Fe decrease on lake formation, as observed here (Figure 4a). However, in many environments Mn cycling and Fe cycling are tightly coupled, where steep redox gradients exist on small scales.[55] Our data could

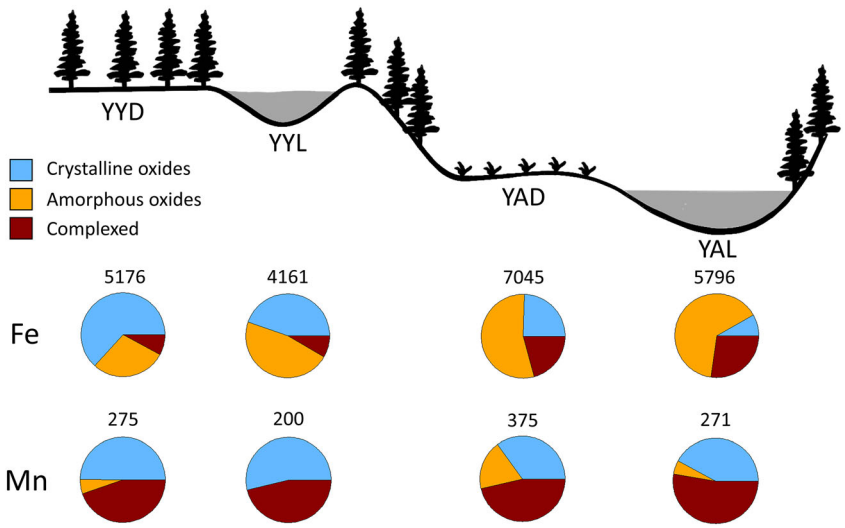

FIGURE 8 Proportion of crystalline oxides, amorphous oxides, and complexed forms of Fe and Mn of the oxide and complexed pool within the sequence of Yukechi cores. These values are based on selective extractions, assuming that the crystalline oxide pool is the difference between DCB (dithionite-citrate-bicarbonate) and oxalate extraction the and amorphous oxide pool is the difference between oxalate- and pyrophosphate extraction. Complexed metals are pyrophosphate extracted. From left to right, cores represent the Yedoma dry (YYD), Yedoma lake (YYL), Alas dry (YAD), and Alas lake (YAL). The size of the total DCB-extracted pool, average in mg kg^{-1}, is given above each pie chart. Al cannot be represented on the same basis because of the higher proportion of oxalate-extracted Al than DCB-extracted Al [Colour figure can be viewed at wileyonlinelibrary.com]

be evidence for the preferential dissolution of Mn phases (relative to Fe phases) on thermokarst lake formation.

Currently, the increase in the number of lakes across the Circum-Arctic region does not offset the land area gained through lake drainage, suggesting that the transition from lake to drained thaw lake basins (i.e., Alas) leads to permafrost aggradation and increasing carbon sequestration.[10] However, future warming, reduced freezing, and potential second lake formation may have a disruptive effect in this trajectory.[10] Lake formation and lake drainage, and their intermediaries, are therefore highly relevant stages of permafrost condition today and in the future. We investigate the influence of the end stages and intermediate stages of thermokarst processes on Fe-OC and Mn–OC interactions and show that drainage and refreezing triggered the increase in absolute and relative concentrations of reactive Fe and Mn phases. In addition, the pool of reactive minerals is higher within the Alas lake than the Yedoma lake core, suggesting an increase in mineral–OC interactions. This suggests that secondary lake formation would have a smaller impact on OC release and subsequent mineralization than initial lake formation. In summary, the increase in reactive Fe and Mn (poorly crystalline oxides and complexes) at the expense of well-crystalline oxides from Yedoma to Alas cores is likely beneficial for OC stabilization.[12,22,95]

5.3 | Changing organo-metallic bindings with the thawing history of ice-rich permafrost deposits

The molar contribution of Ca, Fe, Al, and Mn out of the sum of the complexed phases differs for each metal. On average, this contribution decreases per the sequence Ca, Fe, Al, and Mn, with 80.7%, 13.5%, 3.6%, and 2.2% contribution, respectively. The high contribution of a metal (quantitatively) out of the total complexed metal pool is not the only criterion to prove that this metal is the most influential (qualitatively) on OC binding and protection. Within sediments (all characterized by high pH), we found that Ca is the dominant contributor for organo-metallic complexes. The high Ca concentration within these deposits and the poor solubility of Fe (III) under circumneutral pH might explain the higher contribution of Ca compared to Fe. However, organo-metallic complexes can involve both Fe (II) and Fe (III), and the reported co-occurrence of Fe (II) and Fe (III) in organic complexes from both oxic and anoxic sediments can explain the substantial role of Fe despite the alkaline pH and reductive conditions within sediments.[96] In addition, we found a strong correlation between Mn_p (a minor player quantitatively compared to Fe_p or Ca_p) and C_p (Figure 7), which emphasizes that Mn is likely an important player qualitatively to associate with C and increase its stabilization.

The saturation of functional groups within soluble organic acids can be studied by the metal to C molar ratio, that is, the ratio between the sum of pyrophosphate-extracted metals (Fe_p, Mn_p, Al_p, and Ca_p) and pyrophosphate-extracted C (C_p).[97–99] As described by Boudot et al,[100] organo-metallic complexes that exhibit a low metal to C molar ratio are easily biodegraded because of the lack of significant protective effect. In short, the higher the metal to C molar ratio, the better protected the organic matter may be against microbial degradation. In the Yedoma dry (YYD) core, the metal to C molar ratio is ~0.1. On thermokarst process, this molar ratio increases, and all other cores (YYL, YAD, and YAL) display a metal to C molar ratio of ~0.3 (Figure 9). Organic acids thus display fewer bindings with metals within the Yedoma dry core compared to other cores. The initial lake formation led to a depletion in complexed C and to a lesser extent in complexed metals (Figure 9b, arrow 1), with a significant shift from metal to C molar ratio from 0.1 to 0.3 ratio line (Figure 9a). The second stage of the thermokarst process (i.e., drainage and refreezing; Figure 9b, arrow 2) led to an increase in both complexed C and complexed metals following the 0.3 ratio line. Finally, the second lake formation had no or a few effects on C and metal molar concentrations compared to the initial lake formation. Complexation between organic acids and metals lowers the solubility of organic acids and therefore their availability to microorganisms.[101] This, in turn, can decrease the susceptibility to biological attack and hinders mineralization of organic molecules.[102] Two hypotheses can explain an increase in metal to C molar ratio: (i) the density of functional groups is constant, and the quantity of metals bound to these functional groups increases, or (ii) polyfunctional groups are saturated with metal cations, but the

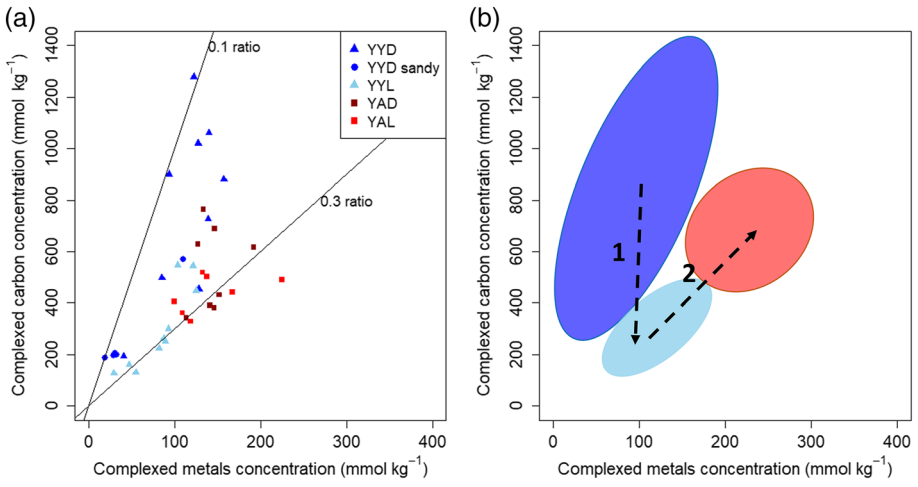

FIGURE 9 (a) Relation between the concentration (in mmol kg^{-1}) of complexed carbon (*y*-axis) and the sum of complexed metals (i.e., Fe, Mn, Al, and Ca) for Yedoma dry (YYD), Yedoma lake (YYL), Alas dry (YAD), and Alas lake (YAL) cores. (b) Conceptual view of the influence of lake formation (1) and lake drainage (2) on complexed mineral and organic phases [Colour figure can be viewed at wileyonlinelibrary.com]

density of the polyfunctional groups increases. The abundance of metal cations (especially Ca) suggests that functional groups are likely saturated and that the second hypothesis is more likely. Either way, the increase in metal to C ratio results in increasing protection for organic acids. Therefore, the increased metal to C ratio observed after thawing of the Yedoma dry deposits likely results in the increase in stability inferred from complexation between metals and OC and to the previous loss of unprotected OC.

Dissolved organic acids have a high density of carboxyl groups (on average 1 carboxyl group for every 10 C atoms; p*K*a ~4–5).[99] For acidic pH, where we found a dominance of a carboxylic polyfunctional group,[103] organic acids are thus considered saturated around a metal to C molar ratio of 0.1. Here, the high pH (mean: ~8–9) allows the presence of other functional groups such as phenolic groups (p*K*a ~10).[104] Advanced stages of organic matter degradation and subsequent depolymerization and oxidation can also lead to the increase in the abundance of polar functional groups and enhance their chemical reactivity toward metal cations and mineral surfaces.[56] Polyvalent cations (i.e., $Fe^{3+/2+}$, Al^{3+}, $Mn^{4+/3+/2+}$, and Ca^{2+}) can bind via coordination to those multiple functional groups and form stable organo-metallic complexes. Complexation mechanisms maintain OC stability and slow down its decomposition rate.[105] The increase in metal to C ratio after thawing highlights the increase in metal–C coordination bindings and suggests a higher protective role against microbial mineralization.

5.4 | Implications for greenhouse gas emissions

We have excellent opportunity to combine data on mineral–OC interactions presented in this study with incubation experiments quantifying CO_2 and CH_4 emissions from identical Yedoma lake and Alas lake sediment cores.[70] The cumulative greenhouse gas production after 1 year of incubation was the highest in Yedoma lake sediments and was 3 and 1.5 times lower in Alas lake sediments for CO_2 and CH_4, respectively.[70] The authors concluded that the highest production in Yedoma deposits was likely due to the decomposition of readily bioavailable organic matter and that the lower greenhouse gas production in the nonfrozen Alas lake sediments likely resulted from advanced OM decomposition during Holocene talik development. Higher greenhouse gas emissions were reported in the Yedoma lake core despite the lower total OC content within this core (median YYL: 0.5 wt%) relative to the Alas lake core (median YAL: 0.8 wt%).

We suggest that the increase in stabilizing mechanisms (involving reactive Fe, Mn, Al, and Ca) in the Alas lake core compared to the Yedoma lake core (Figure 8) could also explain the lowest greenhouse

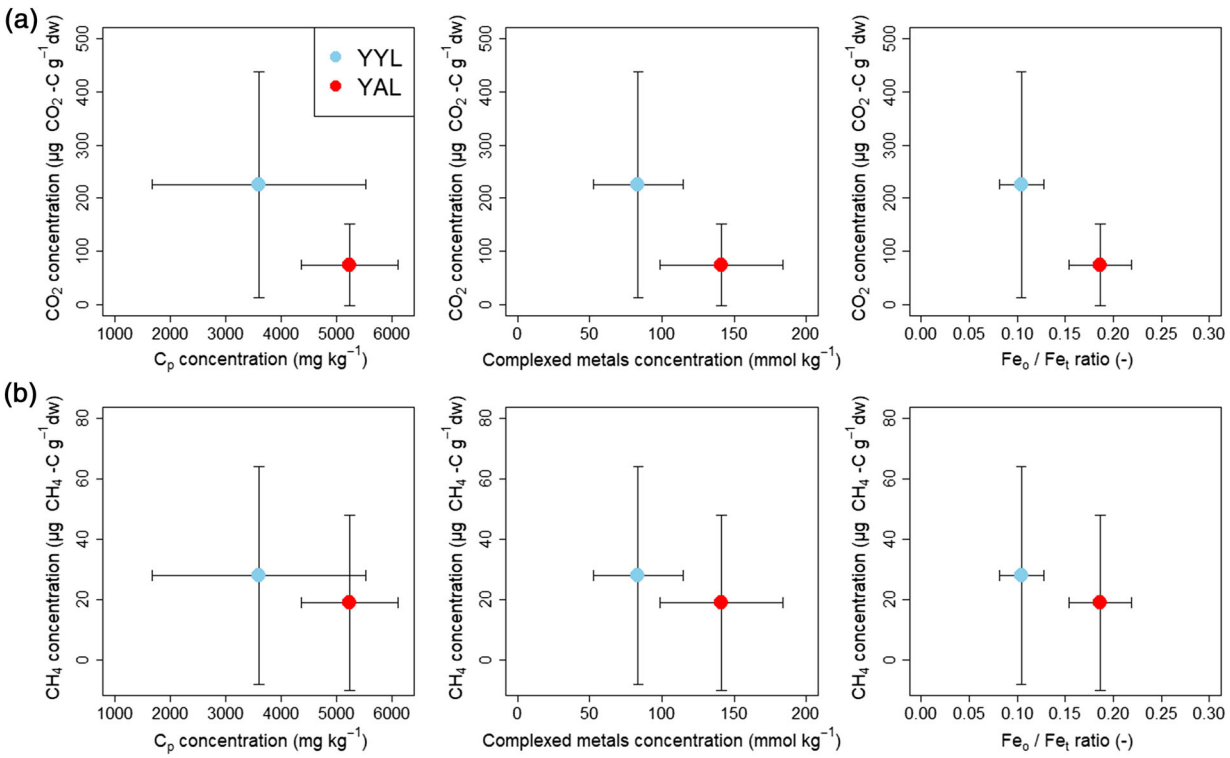

FIGURE 10 Mean and standard deviation of (a) CO_2 (expressed in µg CO_2–C g^{-1} dry weight) and (b) CH_4 (expressed in µg CH_4–C g^{-1} dry weight) emissions on the *y*-axis and mineral stabilization parameters (pyrophosphate-extracted C, sum of complexed metal concentration, and Fe_o/Fe_t ratio) on the *x*-axis for the Yedoma lake sediments (YYL, blue) and the Alas lake sediments (YAL, red). The mean greenhouse gas (CO_2 and CH_4) concentration values are from 1-year (4°C, dark) incubation experiments for Yedoma lake sediments (YYL, $n = 7$) and Alas lake sediments (YAL, $n = 10$).[70,109] No incubation experiments are available in the Yedoma dry and Alas dry sediments to compare with the other cores [Colour figure can be viewed at wileyonlinelibrary.com]

gas production in Alas lake sediments (Figure 10). The lower CO_2 and slightly lower CH_4 production (Figure 10a,b, respectively) in the Alas lake core relative to the Yedoma lake core is concomitant with an increase in both complexed C and sum of the complexed metal concentrations (Figure 10). In addition, the increase in reactive Fe (Fe_o/Fe_t; Figure 10) and reactive Mn, Al, and Ca after first lake drainage (Mn_o/Mn_t, Al_o/Al_t, and Ca_p/Ca_t; Supplementary Figure S13) likely provides better protection for the OC in the sediment. There is also an increase in the total amount of stabilized complexed C on the drainage process, a pool that is kept during the second lake formation (Figure 9b, arrow 2). All these would contribute to the decrease in CO_2 and CH_4 emissions in Alas lake sediments relative to the Yedoma lake sediments. Quantitatively, metals involved in organo-metallic complexes increased by about 70% in the Alas lake relative to the Yedoma lake (83 mmol kg^{-1} in YYL to 141 mmol kg^{-1} in YAL; Figure 10) and may hinder the efficacy of microbial enzymes to degrade OC.[106,107] The amounts of poorly crystallized Fe oxides (Fe_o – Fe_p) almost doubled, from 1.96 g kg^{-1} in the Yedoma lake to 3.74 g kg^{-1} in the Alas lake, on average. Thanks to the high specific surface area of poorly crystallized oxides, iron oxy (hydr)oxides can absorb up to 0.22 g OC g Fe^{-1}.[108] Based on this ratio, Yedoma lake sediments can absorb and protect up to 0.83 g OC kg^{-1} (mean YYL: 3.81 g Fe kg^{-1}) and Alas lake sediments up to 0.93 g OC kg^{-1} (mean YAL: 4.22 g Fe kg^{-1}), which represents a 12% increase.

Overall, we suggest that the shift in the proportion of reactive Fe (from 10.4% in Yedoma lake to 18.6% in Alas lake) and of reactive Mn (from 21.2% in Yedoma lake to 30% in Alas lake) out of their total concentration (also true for reactive Al and Ca; Supplementary Figure S13) might contribute to mitigate CO_2 and CH_4 emissions. In addition, the increased availability of Fe and Mn within the Alas lake core can promote anaerobic oxidation of CH_4.[57,110,111] Under anaerobic conditions, a variety of microorganisms are capable of using Fe and Mn to oxidize CH_4 and mitigate CH_4 emissions.[112,113] The decrease in CH_4 production within the Alas lake core could be explained by an increase in reactive Fe and Mn. Further studies are needed to quantify the direct impact of such mineral OC interactions on methane production rates.

Sediment incubation data and mineral–OC characterization validate the increased attention given to mineral–OC interactions for their potential influence on the permafrost carbon feedback. We demonstrate that the increased abundance in stabilizing surfaces and ions (i.e., via adsorption, coprecipitation, and complexation) led to the decrease in microbial degradation and potentially to methanogenesis inhibition. Although many other parameters can influence greenhouse gas emissions (carbon quality, quantity, and microbial community diversity), we claim that mineral–OC interactions cannot be ignored. Incubation experiments highlighted the contribution and importance of organo-mineral associations for soil OC sequestration in soils of the Siberian Arctic, with over 50% of soil OC bound to minerals.[84] The potential to increase CO_2 and CH_4 production in ecosystems vulnerable to thermokarst processes could be limited by the increase in reactive metals that enhance OC protection and by the increase in Fe and Mn availability that may inhibit CH_4 production.[57,114] Our data support the overwhelming evidence that mineral–OC interactions are key for a more comprehensive understanding of potential greenhouse gas emissions on recent and future thermokarst processes.

6 | CONCLUSION

This study investigated the role of the reactive metals Fe, Mn, Al, and Ca in mineral–OC interactions along a landscape transect in Central Yakutia from undisturbed Yedoma uplands to drained lake and thermokarst lake sediments from different generations. We quantified the influence of thermokarst lake formation and drainage on mineral–OC interactions. Our main conclusions are as follows:

i. Intermediate stages of thermokarst processes like lake formation and lake drainage largely influenced the interactions between reactive metals and OC. Lake formation decreased the amount of complexed OC by 50% and reactive Mn phases by 33%. Lake drainage (disappearance) and refreezing substantially increased the amount of organic compounds (complexed OC and associated to mineral surfaces) and all reactive metals (Fe, Mn, Al, and Ca). The maximum of reactive metals was found in the Alas dry core (YAD).
ii. Regarding the range of thermokarst processes considered (Yedoma dry [YYD] to Alas lake sediments [YAL]), the amount of complexed Fe phases increased threefold. The amount of amorphous Fe doubled at the expense of crystalline phases that decreased significantly from the Yedoma dry to the Alas lake core (63% of crystalline Fe oxides in the free iron pool in the Yedoma dry [YYD] and 8% in the Alas lake [YAL]). Despite a significant increase in amorphous and complexed Mn concentrations in the Alas dry core (YAD), the amount of reactive Mn remained relatively similar from the Yedoma dry (YYD) to the Alas lake core (YAL). Reactive Al and Ca concentrations increased significantly with the thermokarst lake drainage, whereas lake formation had only a minor influence with a slight decrease in reactive Al and Ca concentrations.
iii. Following thermokarst processes, OC had more opportunity to bind with metal cations, which likely increased the stability of organic matter and mitigate microbial degradation.
iv. The higher proportion of reactive metals and complexed OC in Alas lake deposits (YAL) than in Yedoma lake deposits (YYL) is concomitant with lower CO_2 and CH_4 emissions reported in Alas than in Yedoma deposits from the same cores via incubation experiments.

We found an increase in the supply of stabilizing Fe, Mn, and Al surfaces, especially Fe-oxy (hydr)oxides and Fe, Mn, Al, and Ca cations, providing an increased protection for OC. We found an increase in poorly crystalline oxides and in metal to C bindings within organo-metallic complexes on thermokarst lake drainage and refreezing. All these contributed to the concomitant decrease in CO_2 and CH_4 emission on secondary thawing of Alas deposits. Overall, our

data emphasize the overwhelming evidence that mineral–OC interactions need to be considered in the estimates of future greenhouse gas emissions upon thawing of ice-rich permafrost deposits.

AUTHOR CONTRIBUTIONS

A.M. and S.O. designed and planned the experiment. A.G. and J.L. conducted pXRF and XRD measurements and selective extractions with the help of A.M. E.B.A. conducted pH analysis. J.S., L.L.J., L.S., G.G., and M.U. provided the samples and contributed their expertise on permafrost stratigraphy and the sedimentological history of the sample deposits. H.T., C.H., and M.T. contributed their expertise on metals in permafrost regions. B.P. and A.V. helped with pXRF methodology. A.M., A.G., and J.L. performed data processing. A.M. prepared the manuscript with inputs from all coauthors.

ACKNOWLEDGMENTS

This project received funding from the European Union's Horizon 2020 research and innovation program under grant agreement number 714617 to S.O., and S.O. acknowledges funding from the Fund for Scientific Research FNRS in Belgium (FC69480). Field sample collection was funded by a European Research Council Starting Grant PetaCarb to G.G. as well as Alfred Wegener Institute basic funding. The authors acknowledge the Mineral and Organic Chemical Analysis platform at UCLouvain for conducting chemical analysis. The authors thank Elisabeth Mauclet, Yannick Agnan, and Pierre Delmelle for fruitful discussion. They thank the associate editor and two reviewers for their constructive comments.

DATA AVAILABILITY STATEMENT

The data that support the findings of this study are available in the Supplementary Material of this article.

ORCID

Arthur Monhonval https://orcid.org/0000-0003-0038-182X
Jens Strauss https://orcid.org/0000-0003-4678-4982
Guido Grosse https://orcid.org/0000-0001-5895-2141
Lutz Schirrmeister https://orcid.org/0000-0001-9455-0596
Loeka L. Jongejans https://orcid.org/0000-0002-0383-4567
Mathias Ulrich https://orcid.org/0000-0002-1337-252X
Sophie Opfergelt https://orcid.org/0000-0002-1773-4823

REFERENCES

1. Biskaborn BK, Smith SL, Noetzli J, et al. Permafrost is warming at a global scale. *Nat Commun*. 2019;10(1):264. doi:10.1038/s41467-018-08240-4
2. Koven CD, Ringeval B, Friedlingstein P, et al. Permafrost carbon-climate feedbacks accelerate global warming. *Proc Natl Acad Sci*. 2011;108(36):14769-14774. doi:10.1073/pnas.1103910108
3. Schuur EAG, McGuire AD, Schädel C, et al. Climate change and the permafrost carbon feedback. *Nature*. 2015;520(7546):171-179. doi:10.1038/nature14338
4. IPCC. Summary for Policymakers. In: Masson-Delmotte V, Zhai P, Pirani A, et al., eds. *Climate change 2021: The physical science basis. Contribution of working group I to the sixth assessment report of the intergovernmental panel on climate change*. Cambridge University Press; 2021 In Press.
5. Hugelius G, Strauss J, Zubrzycki S, et al. Estimated stocks of circumpolar permafrost carbon with quantified uncertainty ranges and identified data gaps. *Biogeosciences*. 2014;11(23):6573-6593. doi:10.5194/bg-11-6573-2014
6. Strauss J, Schirrmeister L, Grosse G, et al. Deep Yedoma permafrost: a synthesis of depositional characteristics and carbon vulnerability. *Earth Sci Rev*. 2017;172:75-86. doi:10.1016/j.earscirev.2017.07.007
7. Grosse G, Jones B, Arp C. 8.21 Thermokarst Lakes, Drainage, and Drained Basins. In: *Treatise on geomorphology*. Elsevier; 2013:325-353. doi:10.1016/B978-0-12-374739-6.00216-5.
8. Schirrmeister L, Froese D, Tumskoy V, Grosse G, Wetterich S. Yedoma: Late Pleistocene ice-rich syngenetic permafrost of Beringia. In: *Encyclopedia of quaternary science*. 2nd ed. Elsevier; 2013:542-552. doi:10.1016/B978-0-444-53643-3.00106-0.
9. Strauss J, Laboor S, Schirrmeister L, et al. Circum-Arctic map of the Yedoma permafrost domain. *Front Earth Sci*. 2021;9:758360. doi:10.3389/feart.2021.758360
10. Jones BM, Grosse G, Farquharson LM, et al. Lake and drained lake basin systems in lowland permafrost regions. *Nat Rev Earth Environ*. 2022;3(1):85-98. doi:10.1038/s43017-021-00238-9
11. Schneider von Deimling T, Grosse G, Strauss J, et al. Observation-based modelling of permafrost carbon fluxes with accounting for deep carbon deposits and thermokarst activity. *Biogeosciences*. 2015;12(11):3469-3488. doi:10.5194/bg-12-3469-2015
12. Kleber M, Eusterhues K, Keiluweit M, Mikutta C, Mikutta R, Nico PS. Mineral–Organic Associations: Formation, Properties, and Relevance in Soil Environments. In: *Advances in agronomy*. Elsevier; 2015:1-140. doi:10.1016/bs.agron.2014.10.005.
13. von Lützow M, Kogel-Knabner I, Ekschmitt K, et al. Stabilization of organic matter in temperate soils: mechanisms and their relevance under different soil conditions - a review. *Eur J Soil Sci*. 2006;57(4):426-445. doi:10.1111/j.1365-2389.2006.00809.x
14. Opfergelt S. The next generation of climate model should account for the evolution of mineral-organic interactions with permafrost thaw. *Environ Res Lett*. 2020;15(9):091003. doi:10.1088/1748-9326/ab9a6d
15. Dutta K, Schuur EAG, Neff JC, Zimov SA. Potential carbon release from permafrost soils of northeastern Siberia. *Glob Chang Biol*. 2006;12(12):2336-2351. doi:10.1111/j.1365-2486.2006.01259.x
16. Gentsch N, Mikutta R, Shibistova O, et al. Properties and bioavailability of particulate and mineral-associated organic matter in Arctic permafrost soils, lower Kolyma region, Russia: organic matter stabilization in permafrost soils. *Eur J Soil Sci*. 2015b;66(4):722-734. doi:10.1111/ejss.12269
17. Hemingway JD, Rothman DH, Grant KE, et al. Mineral protection regulates long-term global preservation of natural organic carbon. *Nature*. 2019;570(7760):228-231. doi:10.1038/s41586-019-1280-6
18. Kögel-Knabner I, Guggenberger G, Kleber M, et al. Organo-mineral associations in temperate soils: integrating biology, mineralogy, and organic matter chemistry. *J Plant Nutr Soil Sci*. 2008;171(1):61-82. doi:10.1002/jpln.200700048
19. Kramer MG, Chadwick OA. Climate-driven thresholds in reactive mineral retention of soil carbon at the global scale. *Nat Clim Change*. 2018;8(12):1104-1108. doi:10.1038/s41558-018-0341-4
20. Mikutta R, Mikutta C, Kalbitz K, Scheel T, Kaiser K, Jahn R. Biodegradation of forest floor organic matter bound to minerals via different binding mechanisms. *Geochim Cosmochim Acta*. 2007;71(10):2569-2590. doi:10.1016/j.gca.2007.03.002
21. Torn MS, Trumbore SE, Chadwick OA, Vitousek PM, Hendricks DM. Mineral control of soil organic carbon storage and turnover. *Nature*. 1997;389(6647):170-173. doi:10.1038/38260
22. Wagai R, Mayer LM, Kitayama K, Shirato Y. Association of organic matter with iron and aluminum across a range of soils determined

via selective dissolution techniques coupled with dissolved nitrogen analysis. *Biogeochemistry*. 2013;112(1-3):95-109. doi:10.1007/s10533-011-9652-5
23. Eusterhues K, Wagner FE, Häusler W, et al. Characterization of Ferrihydrite-soil organic matter Coprecipitates by X-ray diffraction and Mössbauer spectroscopy. *Environ Sci Technol*. 2008;42(21):7891-7897. doi:10.1021/es800881w
24. Huang W, Hall SJ. Elevated moisture stimulates carbon loss from mineral soils by releasing protected organic matter. *Nat Commun*. 2017;8(1):1-10. doi:10.1038/s41467-017-01998-z
25. Schwertmann U. Solubility and dissolution of iron oxides. *Plant and Soil*. 1991;130(1-2):1-25. doi:10.1007/BF00011851
26. Zhao Q, Adhikari D, Huang R, et al. Coupled dynamics of iron and iron-bound organic carbon in forest soils during anaerobic reduction. *Chem Geol*. 2017;464:118-126. doi:10.1016/j.chemgeo.2016.12.014
27. Wang X, Toner BM, Yoo K. Mineral vs. organic matter supply as a limiting factor for the formation of mineral-associated organic matter in forest and agricultural soils. *Sci Total Environ*. 2019;692:344-353. doi:10.1016/j.scitotenv.2019.07.219
28. Fritsch E, Allard T, Benedetti MF, et al. Organic complexation and translocation of ferric iron in podzols of the Negro River watershed. Separation of secondary Fe species from Al species. *Geochim Cosmochim Acta*. 2009;73(7):1813-1825. doi:10.1016/j.gca.2009.01.008
29. Inagaki TM, Possinger AR, Grant KE, et al. Subsoil organo-mineral associations under contrasting climate conditions. *Geochim Cosmochim Acta*. 2020;270:244-263. doi:10.1016/j.gca.2019.11.030
30. Mikutta C, Wiederhold JG, Cirpka OA, Hofstetter TB, Bourdon B, Gunten UV. Iron isotope fractionation and atom exchange during sorption of ferrous iron to mineral surfaces. *Geochim Cosmochim Acta*. 2009;73(7):1795-1812. doi:10.1016/j.gca.2009.01.014
31. Fiedler S, Sommer M. Water and redox conditions in wetland soils—their influence on Pedogenic oxides and morphology. *Soil Sci Soc Am J*. 2004;68(1):326, 335-335. doi:10.2136/sssaj2004.3260
32. Kögel-Knabner I, Amelung W, Cao Z, et al. Biogeochemistry of paddy soils. *Geoderma*. 2010;157(1-2):1-14. doi:10.1016/j.geoderma.2010.03.009
33. Pan Y, Koopmans GF, Bonten LTC, et al. Influence of pH on the redox chemistry of metal (hydr)oxides and organic matter in paddy soils. *J Soil Sediment*. 2014;14(10):1713-1726. doi:10.1007/s11368-014-0919-z
34. Xue B, Huang L, Huang Y, et al. Roles of soil organic carbon and iron oxides on aggregate formation and stability in two paddy soils. *Soil Tillage Res*. 2019;187:161-171. doi:10.1016/j.still.2018.12.010
35. Barber A, Brandes J, Leri A, et al. Preservation of organic matter in marine sediments by inner-sphere interactions with reactive iron. *Sci Rep*. 2017;7(1):366. doi:10.1038/s41598-017-00494-0
36. Eglinton TI. A rusty carbon sink. *Nature*. 2012;483(7388):165-166. doi:10.1038/483165a
37. Lalonde K, Mucci A, Ouellet A, Gélinas Y. Preservation of organic matter in sediments promoted by iron. *Nature*. 2012;483(7388):198-200. doi:10.1038/nature10855
38. Fiedler S, Wagner D, Kutzbach L, Pfeiffer E-M. Element redistribution along hydraulic and redox gradients of low-centered polygons, Lena Delta, northern Siberia. *Soil Sci Soc Am J*. 2004;68(3):1002-1011. doi:10.2136/sssaj2004.1002
39. Herndon E, AlBashaireh A, Singer D, Roy Chowdhury T, Gu B, Graham D. Influence of iron redox cycling on organo-mineral associations in Arctic tundra soil. *Geochim Cosmochim Acta*. 2017;207:210-231. doi:10.1016/j.gca.2017.02.034
40. Herndon, E., Kinsman-Costello, L., Godsey, S., 2020. *Biogeochemical cycling of redox-sensitive elements in permafrost-affected ecosystems*, in: Dontsova, K., Balogh-Brunstad, Z., Le Roux, G. (Eds.), Geophysical Monograph Series. Wiley, pp. 245–265. 10.1002/9781119413332.ch12
41. Joss H, Patzner MS, Maisch M, Mueller CW, Kappler A, Bryce C. Cryoturbation impacts iron-organic carbon associations along a permafrost soil chronosequence in northern Alaska. *Geoderma*. 2022;413:115738. doi:10.1016/j.geoderma.2022.115738
42. Lim AG, Loiko SV, Pokrovsky OS. Sizable pool of labile organic carbon in peat and mineral soils of permafrost peatlands, western Siberia. *Geoderma*. 2022b;409:115601. doi:10.1016/j.geoderma.2021.115601
43. Monhonval A, Strauss J, Mauclet E, et al. Iron redistribution upon Thermokarst processes in the Yedoma domain. *Front Earth Sci*. 2021b;9:629. doi:10.3389/feart.2021.703339
44. Mu CC, Zhang TJ, Zhao Q, et al. Soil organic carbon stabilization by iron in permafrost regions of the Qinghai-Tibet plateau. *Geophys Res Lett*. 2016;43(19):10,286-10,10294. doi:10.1002/2016GL070071
45. Patzner MS, Mueller CW, Malusova M, et al. Iron mineral dissolution releases iron and associated organic carbon during permafrost thaw. *Nat Commun*. 2020;11(1):6329. doi:10.1038/s41467-020-20102-6
46. Sowers TD, Wani RP, Coward EK, et al. Spatially resolved Organo-mineral interactions across a permafrost Chronosequence. *Environ Sci Technol*. 2020;54(5):2951-2960. doi:10.1021/acs.est.9b06558
47. Bartlett RJ, Ross DS. Chemistry of Redox Processes in Soils. In: *Chemical processes in soils*. John Wiley & Sons, Ltd; 2005:461-487. doi:10.2136/sssabookser8.c9.
48. Johnson K, Purvis G, Lopez-Capel E, et al. Towards a mechanistic understanding of carbon stabilization in manganese oxides. *Nat Commun*. 2015;6(1):7628. doi:10.1038/ncomms8628
49. Li H, Santos F, Butler K, Herndon E. A critical review on the multiple roles of manganese in stabilizing and destabilizing soil organic matter. *Environ Sci Technol*. 2021;55(18):12136-12152. doi:10.1021/acs.est.1c00299
50. Oldham VE, Mucci A, Tebo BM, Luther GW. Soluble Mn (III)–L complexes are abundant in oxygenated waters and stabilized by humic ligands. *Geochim Cosmochim Acta*. 2017;199:238-246. doi:10.1016/j.gca.2016.11.043
51. Rowley MC, Grand S, Verrecchia ÉP. Calcium-mediated stabilisation of soil organic carbon. *Biogeochemistry*. 2018;137(1-2):27-49. doi:10.1007/s10533-017-0410-1
52. Grant KE, Galy VV, Haghipour N, Eglinton TI, Derry LA. Persistence of old soil carbon under changing climate: the role of mineral-organic matter interactions. *Chem Geol*. 2022;587:120629. doi:10.1016/j.chemgeo.2021.120629
53. Schmidt MWI, Torn MS, Abiven S, et al. Persistence of soil organic matter as an ecosystem property. *Nature*. 2011;478(7367):49-56. doi:10.1038/nature10386
54. Ernakovich JG, Lynch LM, Brewer PE, Calderon FJ, Wallenstein MD. Redox and temperature-sensitive changes in microbial communities and soil chemistry dictate greenhouse gas loss from thawed permafrost. *Biogeochemistry*. 2017;134(1–2):183-200. doi:10.1007/s10533-017-0354-5
55. Kappler A, Bryce C, Mansor M, Lueder U, Byrne JM, Swanner ED. An evolving view on biogeochemical cycling of iron. *Nat Rev Microbiol*. 2021;19(6):360-374. doi:10.1038/s41579-020-00502-7
56. Kleber M, Bourg IC, Coward EK, Hansel CM, Myneni SCB, Nunan N. Dynamic interactions at the mineral–organic matter interface. *Nat Rev Earth Environ*. 2021;2(6):402-421. doi:10.1038/s43017-021-00162-y
57. Lipson DA, Zona D, Raab TK, Bozzolo F, Mauritz M, Oechel WC. Water-table height and microtopography control biogeochemical cycling in an Arctic coastal tundra ecosystem. *Biogeosciences*. 2012;9(1):577-591. doi:10.5194/bg-9-577-2012
58. Possinger AR, Bailey SW, Inagaki TM, et al. Organo-mineral interactions and soil carbon mineralizability with variable saturation cycle frequency. *Geoderma*. 2020;375:114483. doi:10.1016/j.geoderma.2020.114483

59. Winkler P, Kaiser K, Thompson A, Kalbitz K, Fiedler S, Jahn R. Contrasting evolution of iron phase composition in soils exposed to redox fluctuations. *Geochim Cosmochim Acta*. 2018;235:89-102. doi:10.1016/j.gca.2018.05.019
60. Wang S, Jia Y, Liu T, Wang Y, Liu Z, Feng X. Delineating the role of calcium in the large-scale distribution of metal-bound organic carbon in soils. *Geophys Res Lett*. 2021;48(10):e2021GL092391. doi:10.1029/2021GL092391
61. Davis CC, Edwards M. Role of calcium in the coagulation of NOM with ferric chloride. *Environ Sci Technol*. 2017;51(20):11652-11659. doi:10.1021/acs.est.7b02038
62. Lim AG, Loiko SV, Kuzmina DM, et al. Organic carbon, and major and trace elements reside in labile low-molecular form in the ground ice of permafrost peatlands: a case study of colloids in peat ice of Western Siberia. *Environ Sci Process Impacts*. 2022a. doi:10.1039/D1EM00547B
63. Ulrich M, Matthes H, Schirrmeister L, et al. Differences in behavior and distribution of permafrost-related lakes in central Yakutia and their response to climatic drivers. *Water Resour Res*. 2017;53(2):1167-1188. doi:10.1002/2016WR019267
64. Melton ED, Swanner ED, Behrens S, Schmidt C, Kappler A. The interplay of microbially mediated and abiotic reactions in the biogeochemical Fe cycle. *Nat Rev Microbiol*. 2014;12(12):797-808. doi:10.1038/nrmicro3347
65. Climate-data.org. Climate data for cities worldwide [WWW Document]. 2022. https://en.climate-data.org/asia/russian-federation/sakha-republic/yakutsk-1806/
66. Gorokhov AN, Fedorov AN. Current trends in climate change in Yakutia. *Geogr Nat Resour*. 2018;39(2):153-161. doi:10.1134/S1875372818020087
67. Soloviev PA. Cryolithic zone of the northern part of Lena-Amga interfluve. *Izd Akad SSSR*. 1959;142.
68. Tarasenko TV. Interannual variations in the areas of thermokarst lakes in central Yakutia. *Water Resour*. 2013;40(2):111-119. doi:10.1134/S0097807813010107
69. Ulrich M, Jongejans LL, Grosse G, et al. Geochemistry and weathering indices of Yedoma and alas deposits beneath Thermokarst Lakes in central Yakutia. *Front Earth Sci*. 2021;9:701. doi:10.3389/feart.2021.704141
70. Jongejans LL, Liebner S, Knoblauch C, et al. Greenhouse gas production and lipid biomarker distribution in Yedoma and alas thermokarst lake sediments in eastern Siberia. *Glob Chang Biol*. 2021b;27(12):2822-2839. doi:10.1111/gcb.15566
71. Windirsch T, Grosse G, Ulrich M, et al. Organic carbon characteristics in ice-rich permafrost in alas and Yedoma deposits, central Yakutia, Siberia. *Biogeosciences*. 2020;17(14):3797-3814. doi:10.5194/bg-17-3797-2020
72. Page AL, Miller RH, Keeney DR. Methods of soil analysis; part 2. Chemical and microbiological properties. *Am Soc Agron Publ*. 1982;363-364.
73. International Centre for Diffraction Data. Be confident with pdf2. 2013. http://www.icdd.com/products/technicalbulletins/PDF-2_Technical_%20Bulletin.pdf. (accessed 5 August 2015).
74. Monhonval A, Mauclet E, Pereira B, et al. Mineral element stocks in the Yedoma domain: a novel method applied to ice-rich permafrost regions. *Front Earth Sci*. 2021a;9:773. doi:10.3389/feart.2021.703304
75. Ravansari R, Wilson SC, Tighe M. Portable X-ray fluorescence for environmental assessment of soils: not just a point and shoot method. *Environ Int*. 2020;134:105250. doi:10.1016/j.envint.2019.105250
76. Mehra OP, Jackson ML. Iron oxide removal from soils and clays by a dithionite-citrate system buffered with sodium bicarbonate. *Clays Clay Miner*. 1960;7(1):317-327. doi:10.1016/B978-0-08-009235-5.50026-7
77. Blakemore LC, Searle PL, Daly BK. Methods for chemical analysis of soils. New Zealand Soil Bureau Scientific Report 10 A, second revision 102. 1981. doi:10.7931/DL1-SBSR-10A
78. Bascomb CL. Distribution of pyrophosphate-extractable Iron and organic carbon in soils of various groups. *J Soil Sci*. 1968;19(2):251-268. doi:10.1111/j.1365-2389.1968.tb01538.x
79. Boiteau RM, Kukkadapu R, Cliff JB, et al. Calcareous organic matter coatings sequester siderophores in alkaline soils. *Sci Total Environ*. 2020;724:138250. doi:10.1016/j.scitotenv.2020.138250
80. Rennert T. Wet-chemical extractions to characterise pedogenic Al and Fe species – a critical review. *Soil Res*. 2019;57(1):1-16. doi:10.1071/SR18299
81. Chao TT. Selective dissolution of manganese oxides from soils and sediments with acidified hydroxylamine hydrochloride. *Soil Sci Soc Am J*. 1972;36(5):764-768. doi:10.2136/sssaj1972.03615995003600050024x
82. Regelink IC, Voegelin A, Weng L, Koopmans GF, Comans RNJ. Characterization of colloidal Fe from soils using field-flow fractionation and Fe K-edge X-ray absorption spectroscopy. *Environ Sci Technol*. 2014;48(8):4307-4316. doi:10.1021/es405330x
83. Cornell RM, Schwertmann U. *The iron oxides: Structure, properties, reactions, occurrences and uses*. John Wiley & Sons; 2003. doi:10.1002/3527602097.
84. Gentsch N, Mikutta R, Alves RJE, et al. Storage and transformation of organic matter fractions in cryoturbated permafrost soils across the Siberian Arctic. *Biogeosciences*. 2015a;12(14):4525-4542. doi:10.5194/bg-12-4525-2015
85. Jakobsen BH, Siegert C, Ostroumov V. Effect of permafrost and palaeo-environmental history on soil formation in the lower Kolyma lowland, Siberia. *Dan J Geogr*. 1996;96(1):40-50. doi:10.1080/00167223.1996.10649375
86. Daly BK. Identification of podzols and podzolised soils in New Zealand by relative absorbance of oxalate extracts of A and B horizons. *Geoderma*. 1982;28(1):29-38. doi:10.1016/0016-7061(82)90038-6
87. R Core Team. R: A language and environment for statistical computing. R Foundation for Statistical Computing, Vienna, Austria. 2018. https://www.R-project.org/
88. Monhonval A, Opfergelt S, Mauclet E, et al. Yedoma domain Mineral Concentrations Assessment (YMCA). 2020. doi:10.1594/PANGAEA.922724
89. Ulrich M, Matthes H, Schmidt J, et al. Holocene thermokarst dynamics in central Yakutia – a multi-core and robust grain-size endmember modeling approach. *Quat Sci Rev*. 2019;218:10-33. doi:10.1016/j.quascirev.2019.06.010
90. Pestryakova LA, Herzschuh U, Wetterich S, Ulrich M. Present-day variability and Holocene dynamics of permafrost-affected lakes in central Yakutia (eastern Siberia) inferred from diatom records. *Quat Sci Rev*. 2012;51:56-70. doi:10.1016/j.quascirev.2012.06.020
91. Hughes-Allen L, Bouchard F, Laurion I, et al. Seasonal patterns in greenhouse gas emissions from thermokarst lakes in central Yakutia (eastern Siberia). *Limnol Oceanogr*. 2021;66(S1):S98-S116. doi:10.1002/lno.11665
92. Schirrmeister L, Dietze E, Matthes H, et al. The genesis of Yedoma ice complex permafrost - grain-size endmember modeling analysis from Siberia and Alaska. *EampG Quat Sci J*. 2020;69(1):33-53. doi:10.5194/egqsj-69-33-2020
93. Schirrmeister L, Wetterich S, Schwamborn G, et al. Heavy and light mineral Association of Late Quaternary Permafrost Deposits in northeastern Siberia. *Front Earth Sci*. 2022;10:741932. doi:10.3389/feart.2022.741932
94. Patrick WH Jr, Jugsujinda A. Sequential reduction and oxidation of inorganic nitrogen, manganese, and Iron in flooded soil. *Soil Sci Soc Am J*. 1992;56(4):1071-1073. doi:10.2136/sssaj1992.03615995005600040011x

95. Chen C, Dynes JJ, Wang J, Sparks DL. Properties of Fe-organic matter associations via Coprecipitation versus adsorption. *Environ Sci Technol*. 2014;48(23):13751-13759. doi:10.1021/es503669u
96. Bhattacharyya A, Schmidt MP, Stavitski E, Martínez CE. Iron speciation in peats: chemical and spectroscopic evidence for the co-occurrence of ferric and ferrous iron in organic complexes and mineral precipitates. *Org Geochem*. 2018;115:124-137. doi:10.1016/j.orggeochem.2017.10.012
97. Nierop KGJJ, Jansen B, Verstraten JM. Dissolved organic matter, aluminium and iron interactions: precipitation induced by metal/carbon ratio, pH and competition. *Sci Total Environ*. 2002;300(1–3):201-211. doi:10.1016/S0048-9697(02)00254-1
98. Schwesig D, Kalbitz K, Matzner E. Effects of aluminium on the mineralization of dissolved organic carbon derived from forest floors. *Eur J Soil Sci*. 2003;54(2):311-322. doi:10.1046/j.1365-2389.2003.00523.x
99. Stevenson FJ. *Humus chemistry: Genesis, composition, reactions*. John Wiley & Sons; 1994.
100. Boudot JP, Hadj AB, Steiman R, Seigle-Murandi F. Biodegradation of synthetic organo-metallic complexes of iron and aluminium with selected metal to carbon ratios. *Soil Biol Biochem*. 1989;21(7):961-966. doi:10.1016/0038-0717(89)90088-6
101. Baldock JA, Skjemstad JO. Role of the soil matrix and minerals in protecting natural organic materials against biological attack. *Org Geochem*. 2000;31(7-8):697-710. doi:10.1016/S0146-6380(00)00049-8
102. Oades JM. The retention of organic matter in soils. *Biogeochemistry*. 1988;5(1):35-70. doi:10.1007/BF02180317
103. Catrouillet C, Davranche M, Dia A, et al. Geochemical modeling of Fe (II) binding to humic and fulvic acids. *Chem Geol*. 2014;372:109-118. doi:10.1016/j.chemgeo.2014.02.019
104. Bell RP. *The proton in chemistry*. Springer Science & Business Media; 2013.
105. Chen Q, Zhang P, Hu Z, et al. Soil organic carbon and geochemical characteristics on different rocks and their significance for carbon cycles. *Front Environ Sci*. 2022;9:666. doi:10.3389/fenvs.2021.784868
106. Kleber M, Sollins P, Sutton R. A conceptual model of organo-mineral interactions in soils: self-assembly of organic molecular fragments into zonal structures on mineral surfaces. *Biogeochemistry*. 2007;85(1):9-24. doi:10.1007/s10533-007-9103-5
107. Mikutta R, Kleber M, Torn MS, Jahn R. Stabilization of soil organic matter: association with minerals or chemical recalcitrance? *Biogeochemistry*. 2006;77(1):25-56. doi:10.1007/s10533-005-0712-6
108. Wagai R, Mayer LM. Sorptive stabilization of organic matter in soils by hydrous iron oxides. *Geochim Cosmochim Acta*. 2007;71(1):25-35. doi:10.1016/j.gca.2006.08.047
109. Jongejans LL, Liebner S, Knoblauch C, Mangelsdorf K, Strauss J. Cumulative greenhouse gas production in thawed sediments underneath a Yedoma and Alas thermokarst lake in Eastern Siberia. 2021a. doi:10.1594/PANGAEA.928140
110. Miller K, Lai C-T, Dahlgren R, Lipson D. Anaerobic methane oxidation in high-Arctic Alaskan peatlands as a significant control on net CH4 fluxes. *Soil Syst*. 2019;3(1):7. doi:10.3390/soilsystems3010007
111. Miller KE, Lai C-T, Friedman ES, Angenent LT, Lipson DA. Methane suppression by iron and humic acids in soils of the Arctic coastal plain. *Soil Biol Biochem*. 2015;83:176-183. doi:10.1016/j.soilbio.2015.01.022
112. Beal EJ, House CH, Orphan VJ. Manganese- and Iron-dependent marine methane oxidation. *Science*. 2009;325(5937):184-187. doi:10.1126/science.1169984
113. Blodau C. Carbon cycling in peatlands — a review of processes and controls. *Environ Rev*. 2002;10:111-134. doi:10.1139/a02-004
114. Bodegom PM, Scholten JCM, Stams AJM. Direct inhibition of methanogenesis by ferric iron. *FEMS Microbiol Ecol*. 2004;49:261-268. doi:10.1016/j.femsec.2004.03.017

SUPPORTING INFORMATION

Additional supporting information can be found online in the Supporting Information section at the end of this article.

How to cite this article: Monhonval A, Strauss J, Thomas M, et al. Thermokarst processes increase the supply of stabilizing surfaces and elements (Fe, Mn, Al, and Ca) for mineral–organic carbon interactions. *Permafrost and Periglac Process*. 2022; 1-18. doi:10.1002/ppp.2162